

Review

Active Optical Beam Shaping Based on Liquid Crystals and Polymer Micro-Structures

Xiaobing Shang ^{1,2,*} , Dieter Cuypers ³ , Tigran Baghdasaryan ⁴ , Michael Vervaeke ⁴, Hugo Thienpont ⁴, Jeroen Beeckman ⁵ , Kristiaan Neyts ⁵ , Quan Li ¹, Chao Wu ^{2,6}, Hongqiang Li ^{2,6}, Changjun Jiang ¹ and Herbert De Smet ^{3,*} 

¹ College of Electronic and Information Engineering, Tongji University, Shanghai 200092, China; 13917311693@163.com (Q.L.); cjjiang@tongji.edu.cn (C.J.)

² Institute of Dongguan-Tongji University, Dongguan 523808, China; chaowu@tongji.edu.cn (C.W.); hqlee@tongji.edu.cn (H.L.)

³ Centre for Microsystems Technology, Ghent University and imec, 9052 Gent, Belgium; dieter.cuypers@ugent.be

⁴ Brussels Photonics Team, Vrije Universiteit Brussel, 1050 Brussel, Belgium; tbaghdas@b-phot.org (T.B.); mvervaeke@b-phot.org (M.V.); hthienpo@vub.ac.be (H.T.)

⁵ Liquid Crystal and Photonics Group, Ghent University, 9052 Gent, Belgium; jeroen.beeckman@ugent.be (J.B.); kristiaan.neyts@ugent.be (K.N.)

⁶ School of Physics Science and Engineering, Tongji University, Shanghai 200092, China

* Correspondence: xiaobing_shang@hotmail.com (X.S.); herbert.desmet@ugent.be (H.D.S.)

Received: 30 September 2020; Accepted: 23 October 2020; Published: 29 October 2020



Abstract: Emerging applications requiring light beam manipulation, such as high-efficiency sunlight concentrators for solar cells, switchable micro-lens arrays for autostereoscopic displays, tunable lenses for augmented reality goggles, auto-focusing spectacles, and smart contact lenses, mostly depend on one or more active optical components with the desired and controllable beam modifying functionalities, preferably manufactured at relatively low cost. Recent progress in research on components based on the combination of liquid crystals (LCs) and various polymer micro-structures is reviewed in this paper. It is found that such components can address the demands appropriately and have the potential of paving the way for large-scale applications of active optical beam shaping components.

Keywords: optical beam shaping; liquid crystals; polymer optical structures; micro-fabrications; adaptive optics

1. Introduction

Through extensive exploration of optical mechanisms and optical technologies over the past four centuries, a series of techniques have been developed for manipulating the propagating direction of a light beam, its intensity distribution, polarization etc. Even nowadays, some of the most basic and simplest components, such as mirrors, lenses and prisms, are still intensively used for various optical beam shaping applications. To realize the controllable beam shaping functionality, conventional optical components usually utilize mechanical motion [1–3]. This approach brings along some serious drawbacks, such as a bulky volume, slow response, high manufacturing cost, frequent maintenance, etc. As technology develops, more and more effective and compact tunable beam shaping solutions have come forward to the domain. Micro-electro-mechanical systems (MEMS) based beam manipulation is among the most promising technologies. One can manipulate a light beam propagation through MEMS controlled micro lenses, micro mirrors, or micro prisms at the micrometer scale [4–10]. However, sophisticated device structures and small device dimensions inhibit their applications in large-area light beam shaping.

Liquid crystals (LCs), usable as tunable electro-optical materials which are compatible with low voltages provided directly by analogue integrated circuits (ICs), demonstrate large and controllable optical anisotropy. Their unique characteristics lead to a dominant position in products of the current display industry, such as thin film transistor (TFT) liquid crystal displays (LCDs). Beside the well-established applications in displays, LCs with their unique electro-optical properties have been the subject of continued research in other application areas, such as LC light intensity attenuators [11–13], LC phase shifters [14–16], LC wavelength selectors [17–19], LC beam shaping devices [20–22] etc. The tunable optical refractive index of LC materials, along with the quite mature LCD fabrication technologies, are reasons to believe that the LC-based beam shaping components have a huge potential to eliminate the disadvantages that are inherent to many existing solutions in the tunable and active optical applications. According to the operation principle, LC beam shaping technologies are mainly based on two schemes: LC gradient refractive index (GRIN) and LC in combination with polymer micro-structures. In the following, recent progress of LC beam shaping components with the two principles is overviewed and discussed.

1.1. Optical Beam Shaping Using LC Gradient Refractive Index

LC-GRIN beam shaping devices rely on gradient variation of the refractive index of an LC layer with a uniform thickness, as is shown in Figure 1. A straightforward solution for realizing the LC-GRIN profile is to use multiple addressing electrodes that are individually driven. The GRIN profile is then directly determined by the electric field profile [23–26]. Good optical performance of the LC beam shaping device requires accurate and fine control of this electric field distribution. This is achieved by using small electrodes with narrow spacing. Often, very complex or even multi-layered electrodes and LC structures are used [27–30]. To simplify the device structure and limit the complexity of driving electronics, resistive or dielectric layers are sometimes deposited in-between the addressing electrodes to smoothen the potential distribution [31–34]. Another way to realize a gradient electric field distribution is to use a constant voltage drop over a layer with a varying dielectric constant profile [35].

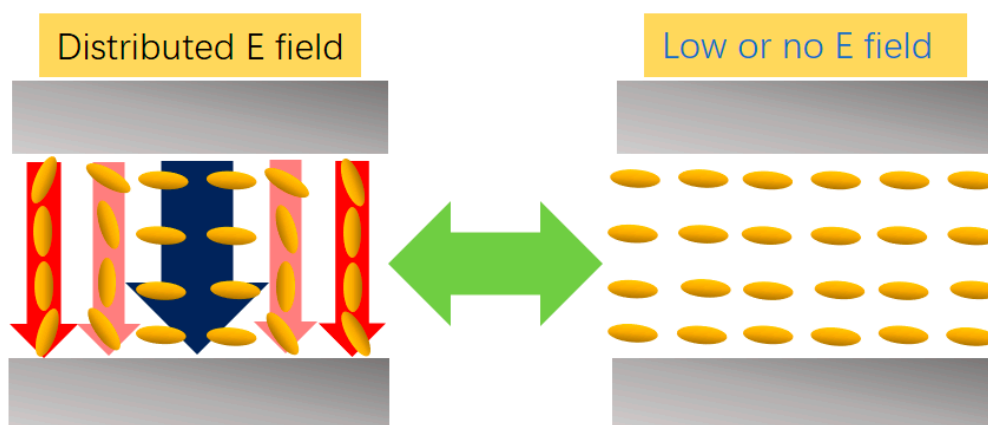


Figure 1. Schematic LC beam shaping devices with a GRIN profile.

Beside the usage of gradient electric fields, other techniques taking advantage of the polymerization are also investigated for the realization of LC-GRIN devices, for example using an ultraviolet (UV) light beam with a Gaussian profile or a grey-scale photomask to induce non-uniform polymerization of the monomers in monomer doped LCs [36,37]. A combination of gradient electric fields with gradient polymerization has also been considered. A narrow UV beam scans over the device containing both LCs and monomers while the applied voltage in the illuminated zone is varied synchronously. A GRIN LC orientation is thus generated by the patterned polymer network. The width of the UV beam line determines the accuracy of the LC GRIN profile [38–41]. Optical scattering induced by the polymer network is still an issue for this technique.

Photonic components based on metamaterials or metasurfaces have attracted much interest in recent years. The dimension, spacing, orientation and composition of the structure units (so-called ‘meta-atoms’) determine the optical properties [42–44]. According to the Pancharatnam–Berry (PB) phase effect, a circularly polarized light beam experiences a phase change of twice the varying azimuthal angle of the anisotropic meta-atoms [45–47]. It is known that nematic LCs are naturally good candidates to be used as the optical meta-atoms. Moreover, since the advent of photo-alignment materials, LC alignment technologies can be implemented in the micron or even submicron scale. Promising results have been reported on active optical LC PB components [48–51]. Those studies usually rely on a patterned UV light beam combined with a linear polarizer to irradiate the photo-alignment layers. Anisotropic photo-chemical reactions in the photo-sensitive layer result in LC orientations with the desired azimuthal angle variations on a (sub)micron scale, leading to the desired optical phase profile. Tunable photonic metasurfaces are realized by introducing transparent electrodes that can influence the LC orientation. The long-term instability of the photo-aligned LC orientation still limits its broad applications.

1.2. Optical Beam Shaping Based on LCs and Shaped Polymer Structures

Beam shaping devices based on the combination of LCs and specially shaped polymer structures, employ the profile of the LC–polymer interface to achieve the desired beam control. One approach utilizes a liquid crystalline polymer (LCP) lens array combined with a tunable polarization converter [52–54]. Photo-curable LC pre-polymer material is filled into the gap between the lens array and the counterpart flat substrate, and aligned along the defined direction. After UV curing, a LC polymer layer forms and it has the same optical property as the aligned LC pre-polymer. The newly generated interface between the LCP layer and the micro lens structure changes the light wavefront, resulting in beam convergence. A 90° twisted nematic LC device is used as a polarization converter to rotate the linear light polarization by 90°. If the light with the orthogonal polarization meets the interface of the aligned LCP layer, there is no beam focusing because the refractive index of the LCP matches that of the micro lens structure.

Other methods adopt nematic LCs rather than LCPs to avoid the complex device architecture and reduce the cost [55–60]. A nematic LC device with micro lens array is schematically shown in Figure 2. Conductive and transparent layers are deposited on both the micro-lens array and the flat counterpart substrate. The LC layer can be switched by applying strong electric fields, leading to a switchable beam shaping compared to the ‘fixed’ one produced by the UV cured LC polymers. To avoid the need for an LC alignment layer, a combination of polymer dispersed or stabilized LCs with micro lens arrays has been proposed [61,62]. Without electric fields, the LC droplets are randomly aligned, exhibiting an average refractive index for the incident light. By applying high voltages, the LC molecules in each droplet are realigned parallel to the electric field. If the LC refractive index matches with the micro lens material at high voltages, the whole device does not modify the incident beam. Without an electric field, the LC device focuses the incident light effectively due to the index mismatch between the LC droplets and the micro lenses.

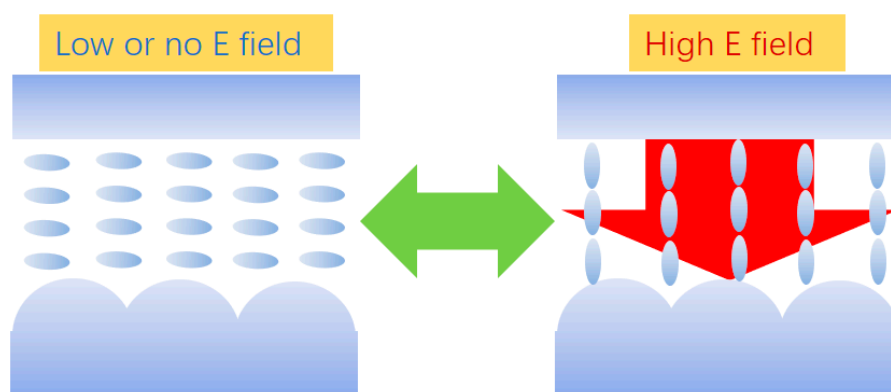


Figure 2. Schematic LC beam shaping device with combination of nematic LCs and optical micro-structures.

1.3. Summary

LC beam shaping components based on the two main mechanisms have their own advantages and disadvantages. The fabrication of LC GRIN devices is more compatible with the current LCD manufacturing process. Moreover, this kind of LC devices usually requires a low operation voltage that can be directly driven by IC drivers. Compared to the LC-GRIN beam shaping devices, the operation voltage of LC–polymer structure based beam shaping devices is relatively large due to the voltage dividing effect of the polymer layer. Nevertheless, this issue can be overcome by using well-designed electronic driving circuits.

For the LC GRIN devices, the spatial LC orientation plays an important role in the optical performance. The gradient refractive index profile of the LC, which is generated by either the spatially varying electric field or the spatially varying polymerization, usually deviates from the ideal one to some extent, resulting in undesired optical effects, such as stray light and light scattering. Imperfections in the refractive index profile can be attributed to the difficulty of device processing, the coupling of electric fringe fields, the continuity of the LC elastomer, the instability of the LC orientation by photo-alignment, etc.

Beam shaping components based on LCs and polymer micro-structures, can take full advantage of the well-developed design methods and tools, as well as advanced fabrication technologies of modern optics, to achieve the best optical property one envisages. Good LC alignment may be difficult to establish within the periodic micro-structures. It is gratifying that the LC alignment in this kind of devices has been proved possible using established technology, such as rubbing alignment, oblique SiO_x evaporation and photo-alignment [63,64].

In the following sections, our discussion will focus on the LC–polymer structure-based beam shaping components, the fabrication technologies of optical micro-structures, various schemes and methods of beam shaping components based on LCs and polymer micro-structures, particularly linear and circular blazed gratings.

2. Fabrication of Optical Micro-Structures

Fabrication of optical micro-structures is the prerequisite for the target LC–polymer structure-based beam shaping components. Four major technologies for fabrication of optical micro-structures will be discussed: diamond tooling, hot embossing, laser ablation and soft lithography. The four processing techniques each have their merit and depending on the circumstances and application can be the most suitable technique to create various optical micro-structures. In the following part of this section, an introduction to the domain, experimental results, merit, and demerits of each technology will be presented.

2.1. Diamond Tooling for Optical Micro-Structures

Conventional optical components are created by means of lapping, milling, and polishing to remove excess material in specific areas with different force toward the abrasive loaded tool [65]. Diamond tooling generates optical structures through moving a tiny diamond tip along the designed path, which approximates the desired surface profile of the optical components. Single point diamond tooling (SPDT) is a computer numerical controlled (CNC) lathe machining process. It uses a natural or synthetic diamond tool with a tip radius ranging from millimeters down to micrometers. In the discussion below, a five-axis SPDT equipment (Nanotech 350FG, Swanzey, NH, USA) has been used to fabricate optical micro-structures.

To realize linear gratings, an efficient way is to install a diamond cutting tip with a cylinder shape onto a high-speed rotational spindle, and mount the workpiece tightly onto the holding stage which is driven accurately in linear motion. This is a typical micro milling process, and the schematic procedure is depicted in Figure 3. Before applying the diamond milling, the whole spindle with the diamond tool has to be inclined toward the sample surface with a certain angle, which corresponds to the blaze

angle of the grating. Through high speed rotation of the diamond tool, as well as the programmed linear motion of the translational stage along the X and Y axis, a micro milling process is applied to the sample surface, creating a triangular groove with a tilted sidewall. Repeating the milling process for each groove, the desired micro grating structures are generated on the sample surface.

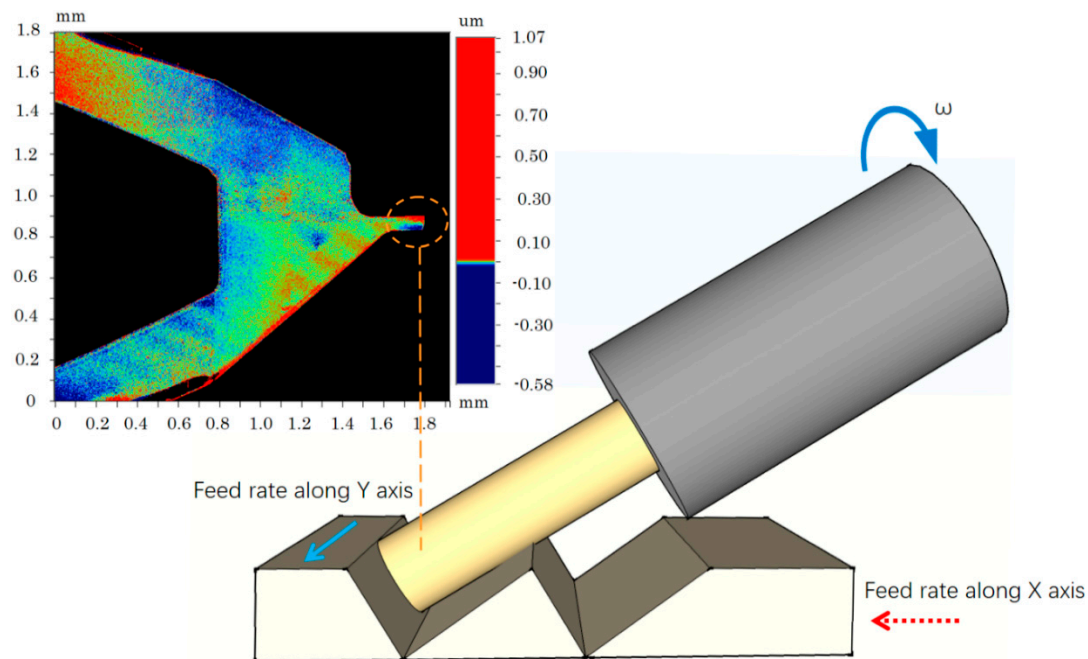


Figure 3. Diamond tooling process for linear micro gratings using a cylindrical diamond tip; the inset represents the surface profile of the cylindrical diamond tip with a radius of 50 μm .

A cylindrical diamond tool with a radius ($r_p = 252 \mu\text{m}$), high spindle speed ($\omega = 40,000 \text{ rpm}$) and moderate feed rate (11 mm/min), are employed to fabricate linear micro grating structures in a copper alloy MS58 ($\text{CuZn}_{39}\text{Pb}_3$). The resulting facet topography is shown in Figure 4a. Normally the average roughness R_a and the root mean square roughness R_q are used to evaluate the surface finish quality. The relationship between the total integrated scatter (TIS) and the root mean square roughness shows that, in order to limit the TIS of an optically transmissive surface to be less than 2%, the required surface roughness R_q needs to be less than $\lambda/8$, which satisfies the surface finish grade A-2 of the Society of the Plastics Industry (SPI) [66]. The surface roughness R_a and R_q shown in Figure 4a are less than $\lambda/8$, demonstrating a good surface finish with high optical quality.

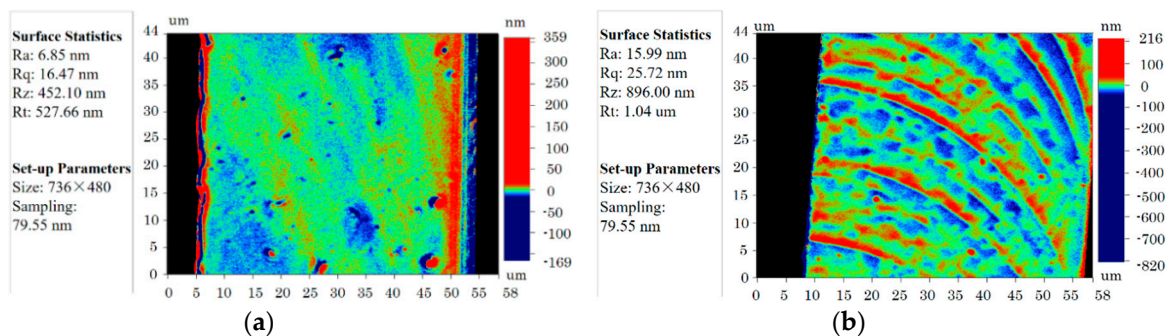


Figure 4. The topography of the grating facet on the slow slope made by diamond milling with a cylindrical diamond tip of (a) $r_p = 252 \mu\text{m}$ and (b) $r_p = 50 \mu\text{m}$; r_p —the radius of the cylindrical diamond tip; R_a —the roughness average; R_q —the root mean square (RMS) roughness; R_t —the maximum height of the surface profile; R_z —the average maximum height of the surface profile.

Another cylindrical diamond tip with a smaller radius is adopted to fabricate the linear grating structures. Its profile is measured by a Wyko NT3300 optical profiler and shown in the inset of Figure 3. The effective length and diameter of this diamond cylinder are about 200 μm and 100 μm , respectively. The cylinder part of the diamond tip plays a key role in the creation of micro grating structures during the milling process. The profile of the grating facet created by the smaller diamond tip is shown in Figure 4b. It is clearly seen that there is a series of grinding traces on the grating facet of the slow slope using the diamond tip with $r_p = 50 \mu\text{m}$. These curved lines are generated by the combination of the rotation of the cylindrical tip and the translational movement along the Y axis, and contribute to the surface roughness. Fortunately, the surface roughness ($R_a = 15.99 \text{ nm}$, $R_q = 25.72 \text{ nm}$) shown in Figure 4b is less than $\lambda/8$ and still satisfies the requirement of a good optical surface.

2.2. Hot Embossing for Optical Micro-Structures

A hot embossing equipment (HEX04, Jenoptik, Jena, Germany) is used to replicate micro patterns from a rigid metal mold onto polymethyl methacrylate (PMMA) layers. The equipment used here is based on the mode of plate to plate (P2P). The metal molds are made by the aforementioned diamond tooling on the copper alloy MS58. The hot embossing process is illustrated in Figure 5. The metal mold is first well installed and loaded onto the sample in a vacuum chamber. The metal mold or/and the bottom loading stage are then heated above the glass transition point (T_g) of the candidate material. An adequate loading force is subsequently applied to the metal mold and kept for a certain duration. After that, the temperature starts decreasing for the demolding. The mold is finally removed from the substrate, forming the micro-structures on the PMMA layers with a reverse shape compared to the master metal mold.

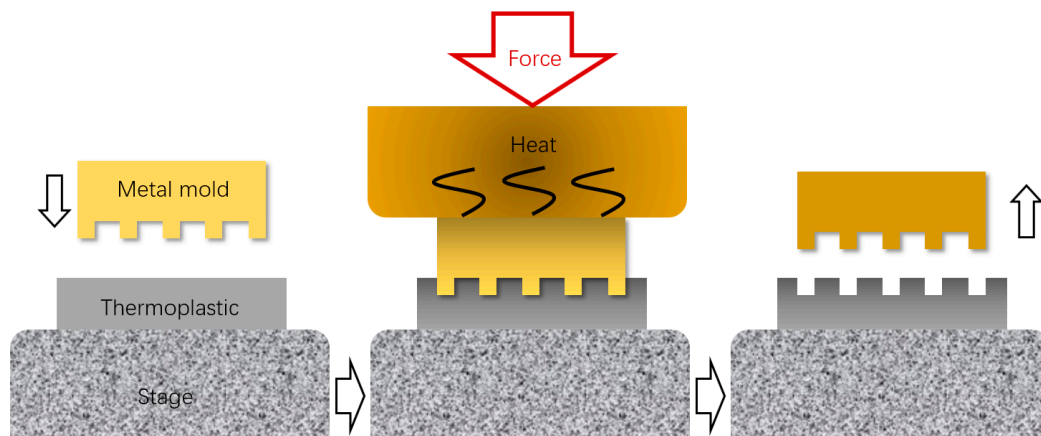


Figure 5. Schematic process flow of hot embossing.

In theory, the polymer layer used for hot embossing must at least be as thick as the required structure height. But in practice, this thickness needs to be several times higher. Polymer layer coated glass or wafer substrates are frequently used for many electro-optical applications. A PMMA layer with a thickness of 21 μm is formed on an indium tin oxide (ITO) coated glass substrate by spin coating. Subsequently, a hot embossing process is applied to the PMMA layer for creating the linear gratings with a pitch of 50 μm and height of 10 μm . The result is shown in Figure 6. Due to the low viscosity and the limited low concentration of the available PMMA/anisole solution, the maximum PMMA thickness obtained by spin coating is about 21 μm . The PMMA samples are hot embossed at different temperatures and loading forces. Figure 6a clearly shows that there is a flat area on top of the grating, which causes a large deviation of the structure from its initial design. Even with a higher temperature, larger force and prolonged press time, the structure is still not adequate (Figure 6b). The reason why hot embossing on the PMMA coated glass is unsuccessful is because the obtained PMMA layer (21 μm

thick) is too thin. The corresponding velocity allowing the flow inside the thin PMMA layer is limited, resulting in incomplete and defective grating structures.

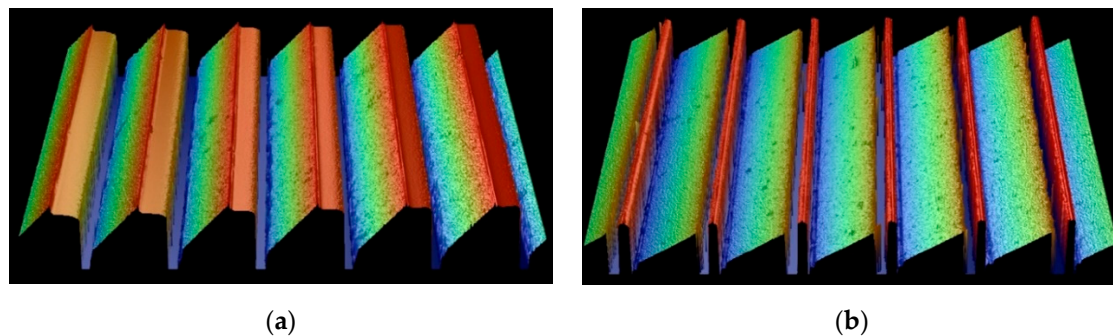


Figure 6. Hot embossed structures on PMMA coated ITO glass with (a) a press force of 20 kN at 145 °C for 120 s; (b) a press force of 25 kN at 165 °C for 200 s.

In order to get good replication from the master mold, bulk PMMA sheets (0.5 mm or 1 mm thick) are hot embossed using an optimized process with 145 °C molding temperature, 2.5 mm/min mold velocity and press force ranging from 15 to 20 kN. Figure 7a shows the 3D profile of the circular micro-structures on PMMA sheets using hot embossing. The measured dimensions are now very close to the designed values. Furthermore, the surface roughness R_a is 50–70 nm, satisfying the optical requirement generally. Linear grating structures are embossed on PMMA sheets as well, and shown in Figure 7b. Their dimensions also approximate the design. Hot embossing on bulk PMMA sheets is proven to be a successful method.

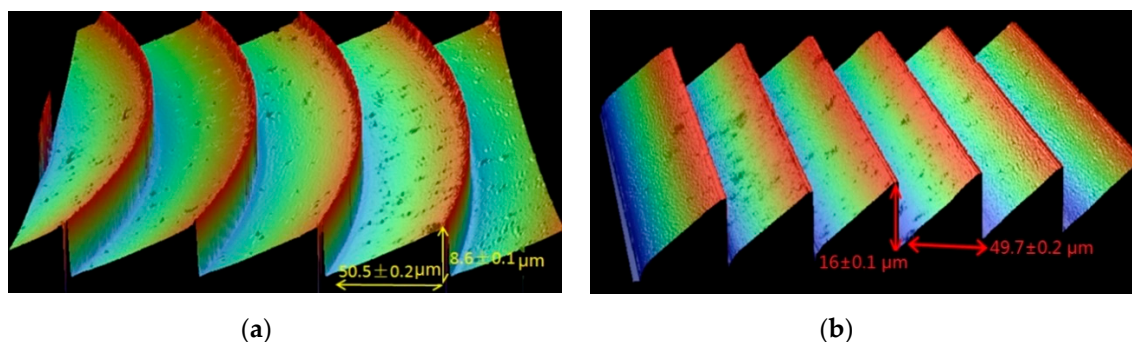


Figure 7. Hot embossed micro-structures on bulk PMMA sheets: (a) circular gratings and (b) linear gratings.

2.3. Laser Ablation for Optical Micro-Structures

Another advanced tool for the fabrication of optical micro-structures is laser ablation. Laser ablation generates specific patterns by direct irradiation of laser pulses onto the polymer surface, resulting in local removal of the material. For laser ablation of polymer materials using an ultra-violet (UV) beam, it is well-established that the first step is the absorption of highly energetic laser photons, resulting in electronic excitation. However, the following steps are still controversial, and three theoretical models are considered: photothermal, photochemical and photophysical. In the photothermal process, the electronic excitation is thermalized on a picosecond timescale, resulting in thermal bond breaking [67,68]. If electronic excitation causes direct breaking of the chemical bonds, it contributes to the photochemical reaction [69,70]. The photophysical model assumes that both the photothermal and the photochemical reactions play a role, whereby the dominating factor in the process depends on the etching conditions and the polymer compositions [71–73]. If laser ablation is used to fabricate optical structures, the thermal heating effect should be minimized, to prevent the polymers from getting charred.

Laser ablation combined with a shadow mask is adopted to create micro grating structures on polymer sheets. The laser beam is shaped by a mask with a triangular aperture and focused on the target polymer substrate that is driven by a translational stage. The polymer surface is subjected to a series of triangle-shaped laser pulses at different positions, resulting in a lateral distribution of the cumulative ablation depth. By repeating the ablation with a certain periodicity, a micro grating structure forms on the polymer surface. The fabricated grating structure will be combined with nematic liquid crystal to build a switchable beam shaping component. The cell gap of a LC device is the distance between the two substrates that confine the liquid crystal. It plays an important role in the optical property, such as the optical uniformity and the response time. Usually, the cell gap is maintained by inserting spherical particles with a well-defined diameter between the two substrates as spacers, but ball spacers have some drawbacks, e.g., balls easily move away from their original positions. The other issue is that ball spacers would sink into the grating valleys and not be able to sustain the cell gap between the two substrates. These problems are detrimental to the optical performance of the LC device. To simplify the fabrication of switchable beam shaping components and overcome the disadvantage of ball spacers, two technologies are developed to build extra structures as spacers on the gratings: overlapping ablation and double mask ablation.

In the overlapping ablation technique (Figure 8), the shaped laser beam is first used to create a triangular groove. During the ablation, specific areas are skipped, where the material retains the original surface. When the same laser beam starts to ablate the adjacent grooves, the laser beams slightly overlaps the already created groove. The obtained grating in between the two grooves has a lower tip than the original surface. The skipped areas which retain their original surface will act as spacers for the cell gap. The resulting grating profile is also shown in Figure 8. The overlapping ablation works well for spacer creation. It only needs a one-time alignment between the shadow mask and the movement of polymer substrates. However, its disadvantage is that the spacer height is not flexible to adjust.

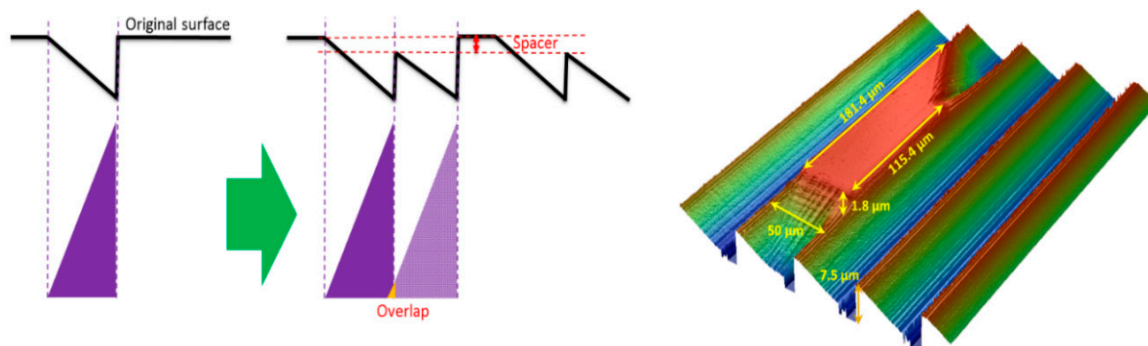


Figure 8. Schematic overlapping laser ablation and the resulting grating with spacer structures. Reproduced with permission [74]. Copyright 2015, IOP Publishing.

Another laser processing technique, the double mask ablation, is developed for the fabrication of spacers built on gratings. The double mask ablation (Figure 9) works by first ablating specific regions with a big rectangular mask, resulting in a height difference between the ablated area and the unablated area. The ablated area is further ablated with another triangular/trapezoidal mask to create the gratings. The depth reached by the first rectangular mask determines the effective spacer height. To produce the desired gratings, sufficient material needs to be left for the subsequent creation of the triangular gratings. Figure 9 shows the 3D profile of the gratings with spacers made by double mask ablation. The unablated areas behave as spacers for the LC beam shaping devices. The double mask ablation needs one more extra alignment between the trace of the first mask and the second mask, however, it can tune the spacer height more flexibly compared to the overlapping ablation.

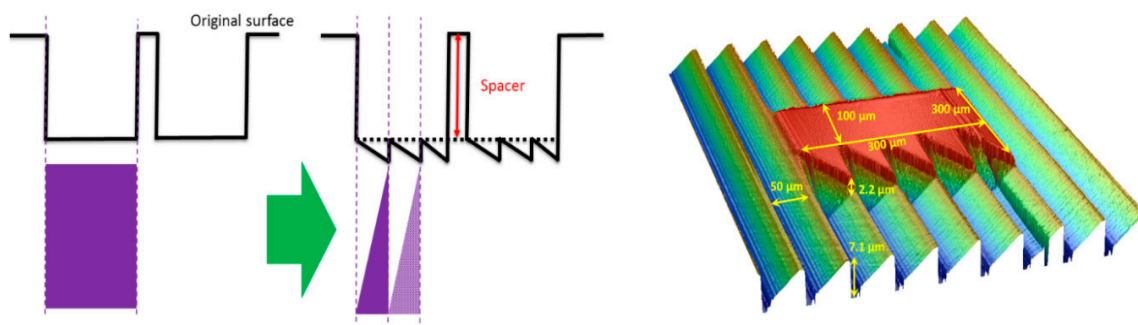


Figure 9. Schematic double mask laser ablation and the resulting grating with spacer structures. Reproduced with permission [74]. Copyright 2015, IOP Publishing.

2.4. Soft Lithography for Optical Micro-Structures

Diamond tooling usually requires a long processing time to fabricate micro-structures, while laser ablation has a moderate processing efficiency. Neither of them is suitable for mass production of large-size and low-cost optical structures. Hot embossing seems promising for the issues, but it is difficult to get complete micro-structures on thin layer coated glass substrates, due to insufficient material for extrusion and filling into the relief pattern of the master mold. Therefore, another processing technique, soft lithography, is developed for the rapid and low-cost replication of polymer micro-structures on glass substrates. As the name indicates, soft lithography utilizes an elastomeric mold or stamp to transfer the micro/nano patterns onto the target substrates, which is the main difference from the aforementioned hot embossing using a rigid mold.

The advantage of using soft and elastic molds is that they can be laminated onto the resin layer, which avoids the formation of bubbles in the replicas. Therefore, gel-like materials such as polydimethylsiloxane (PDMS) are adopted for the mold fabrication. In order to achieve high efficiency of the replication process, UV curing is adopted for the polymerization of optical resins instead of thermal curing. The schematic process flow is shown in Figure 10. After depositing the PDMS pre-curable solution onto the grating master mold, degassing is sometimes necessary to remove encapsulated bubbles. The mold curing can be implemented by using thermal curing or UV curing, depending on the material property. The elastic mold is subsequently peeled off from the master mold. For the imprinting process, a suitable photopolymer layer is deposited on the ITO glass substrate. The soft mold is laminated onto the liquid layer, an UV exposure is applied to the assembly and the resin layer is cured in a short and non-thermal step. The micro grating structures are obtained after the PDMS mold is peeled from the glass substrate. The profiles of the grating structures are shown in Figure 11.

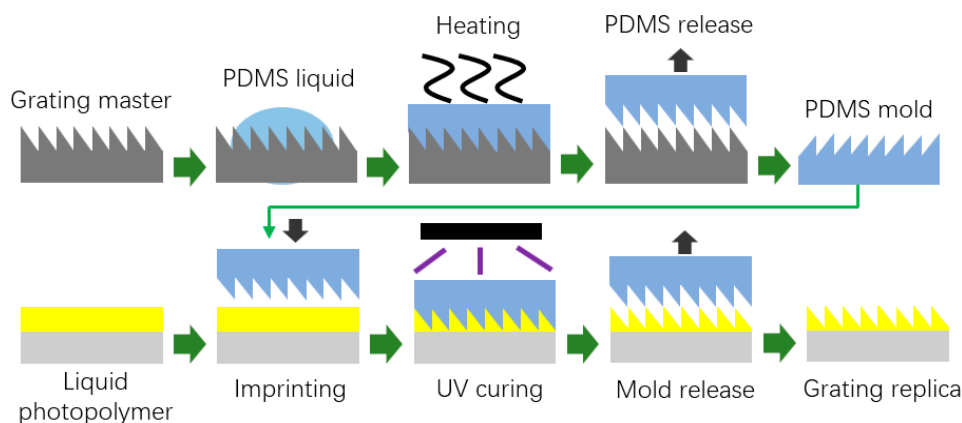


Figure 10. Process flow of soft lithography for optical micro-structures.

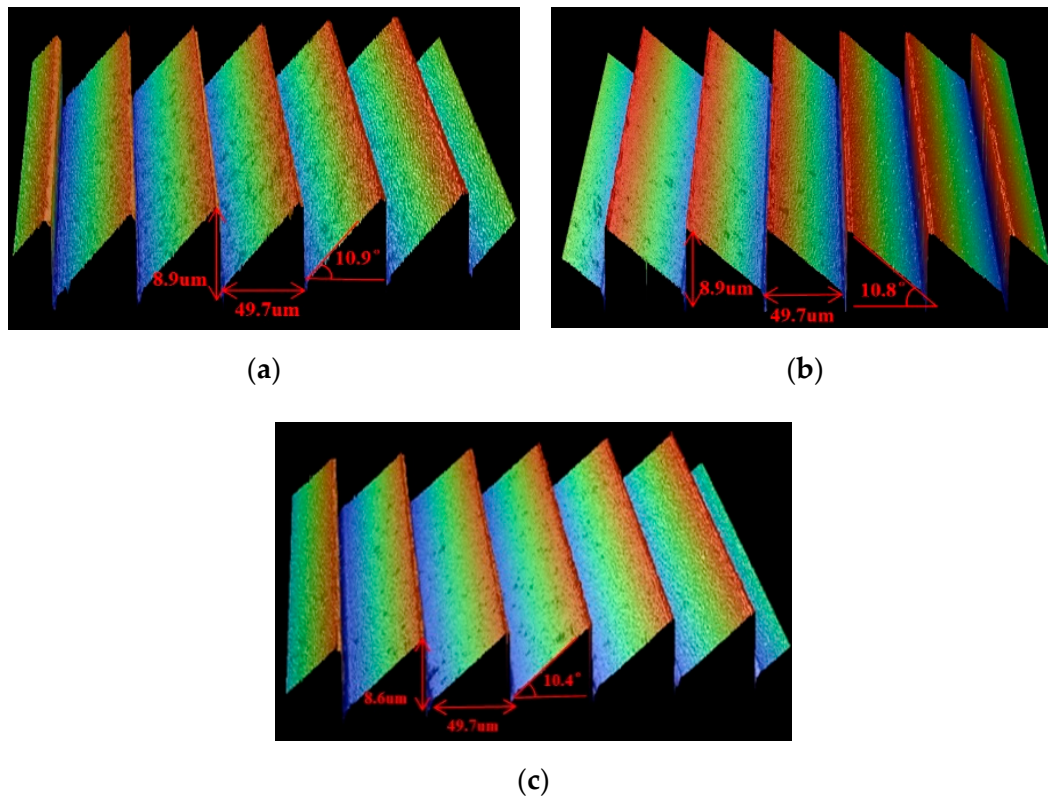


Figure 11. Surface profile characterized by a WYKO surface profiler: (a) master grating on PMMA sheet; (b) negative PDMS mold; (c) NOA 74 grating replica. Reproduced with permission [63]. Copyright 2015, IEEE.

In some cases, it is difficult to create a positive shape for the structure one envisages using diamond tooling or laser machining. For example, to build the ‘fixed’ spacers on gratings, it is easier to use laser ablation or diamond tooling to cut an extra dent at the groove bottom. If the pattern is reversed, the fixed spacer appears on top of the grating structures. Therefore, creating a master mold with a negative shape and introducing an extra transfer step is a solution for this kind of challenge. Realization of soft molds having a similar negative shape as the original master is a prerequisite, as it will be used as a replication mold for the subsequent soft lithography process. Silicone molds with the same shape as the master have been realized using the double silicone replication process [75]. Without releasing agent, the risk of cross-polymerization between the casted silicone liquid and the formed silicone mold still exists for most of the silicone materials. The usage of an extra thin releasing layer changes the dimension of the second silicone replica unavoidably [76]. The basic idea here is to use an UV curable polymer or resin, which has a large elastic modulus but weak adhesion strength to the PMMA sheet, to form a reversed grating structure from the PMMA master with a negative shape. This positive polymer mold will act as a new master mold for the subsequent process. Here the UV curable glue NOA 68 (Norland Products Inc., Cranbury, NJ, USA) is adopted to fabricate this positive polymer mold. The whole process is shown in Figure 12. After dispensing the NOA 68 glue on the negative PMMA master, the glue layer is UV cured and easily peeled off without any damage due to its good elasticity and weak adhesion to the PMMA sheet. The Sylgard[®]184 silicone is then deposited on the polymer mold by spin coating and cured in the convection oven at a low temperature. After peeling off the PDMS mold having the same shape as the original PMMA master, it can be used for the reverse replication of circular micro gratings on glass substrates as described in the above section.

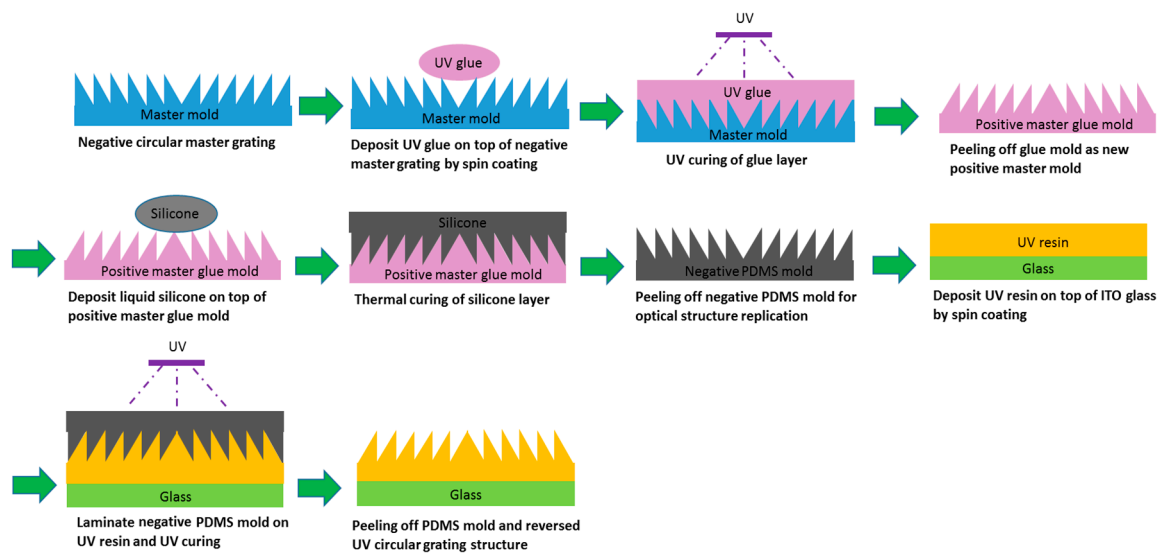


Figure 12. Replicating circular micro grating structure with a reversed shape by the polymer-PDMS replication. Reproduced with permission [77]. Copyright 2016, IOP Publishing.

2.5. Summary

Four different technologies for the fabrication of optical micro-structures are implemented in the study. To give readers a direct impression of those technologies, their key characteristics are summarized in Table 1. From this table, it can be concluded that diamond tooling and laser ablation are more suitable for the master mold fabrication, while hot embossing and soft lithography are better for the massive replication of optical micro-structures. Hot embossing is more adequate to structure replications on bulky thermoplastic polymer sheets, while soft lithography excels in micro/nano structure replications on thin layer coated glass/wafer substrates.

Table 1. Comparison of different fabricating technologies for optical micro-structures.

Name	Material	Efficiency	Merit	Demerit
diamond tooling	non-ferrous	low	free-form optical structures	complex control & alignment
laser ablation	polymers	medium	simple setup	charring effect & periodic defects
hot embossing	thermoplastics	high	Efficient & easy process	high temperature & large loading force
soft lithography	liquid adhesives	high	high efficiency & broad adhesives	still in development for mass production

3. LC-Polymer Grating Based Beam Shaping Components

The micro-grating structures made by the aforementioned techniques are combined with liquid crystals to realize beam shaping components with various functionalities: linear gratings combining with nematic LCs have achieved one dimensional and continuous beam deflection; beam broadening and beam condensing is respectively fulfilled by using circular micro-grating structures and nematic LCs; polarization independent beam shaping is realized by adopting dual frequency cholesteric LC (Ch-LC) mode; dual driving scheme based on dual frequency nematic LC is employed to obtain fast switching beam shaping components; fast response blue phase (BP) LC beam deflecting devices have also been attained with a combination of BP LCs and linear micro-grating structures.

3.1. Beam Deflection Using a Nematic LC-Linear Grating Device

Linear micro grating structures are combined with nematic LCs to realize one dimensional beam deflection. LC alignment plays an important role in the optical performance of the device. It is even more difficult in the beam shaping device due to the influence of the micro-structures. Several different alignment technologies are applied to the LC-polymer grating device: velvet rubbing, oblique SiO₂ evaporation and photo-alignment. The LC textures of beam shaping devices using different alignment techniques are observed under a crossed-polarizer microscope, as shown in Figure 13. It is seen that the LC orientations are all aligned along the micro groove direction. The rubbing technique employs a rotatable roller covered with a velvet to pass through the substrate surface. Tiny and invisible patterns (with scratch width around 200 nm or below, scratch depth of tens of nanometers or below) are created on the surface [78]. The LC molecules are anchored in a way that the LC long axis is aligned along the grating groove direction in the beam steering device. This process sometimes results in damages or defects on the non-flat surface, as shown in Figure 13a. Therefore, two non-contact alignment methods (oblique SiO₂ evaporation and photo-alignment) based on inorganic and organic materials, respectively, are developed to avoid the issues induced by the rubbing scheme. Oblique SiO₂ evaporation utilizes the induced dipole to dipole interactions based on Van der Waals force between the obliquely evaporated SiO₂ layer and the LC molecules [79–82]. Photo-alignment on the other hand makes use of the anisotropic interaction between the photo sensitive material and the LC layer [83–85]. Both methods are able to achieve good LC alignment within the linear grating structures, as shown in Figure 13b,c.

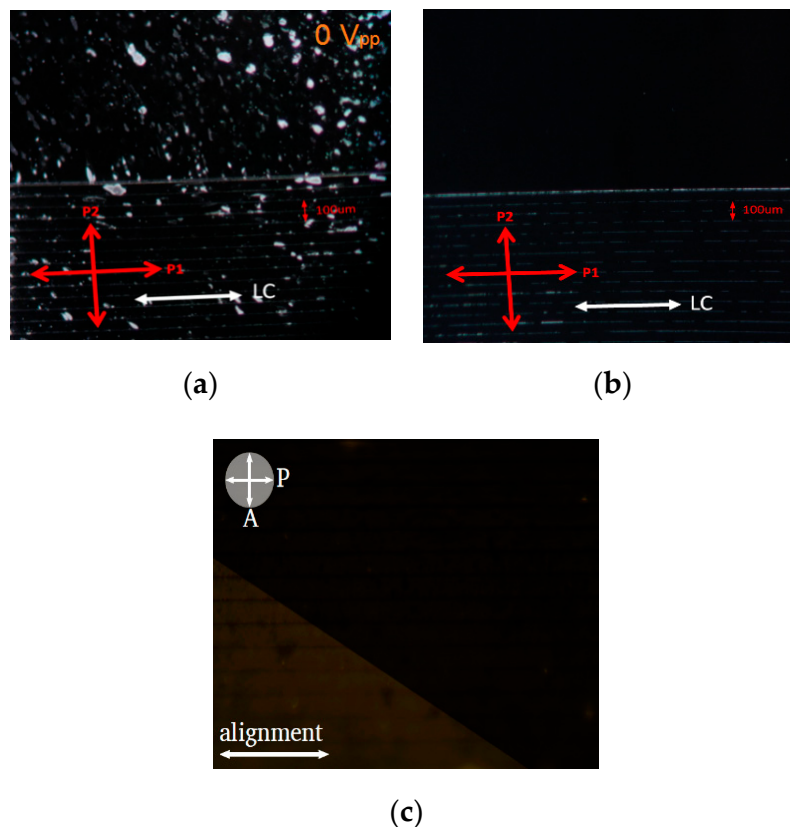


Figure 13. LC textures within the LC-micro grating devices by different alignment technologies: (a) velvet rubbing; (b) oblique SiO₂ evaporation; (c) photo-alignment. Reproduced with permission [63], copyright 2015, IEEE; reproduced with permission [64], copyright 2016, OSA.

After the linear gratings are treated by the alignment technologies and assembled with their aligned counterpart ITO substrates, the nematic LC-E7 is filled into the empty cell. Beam deflecting device with

one dimensional beam shaping is finally generated. Its device architecture is demonstrated in Figure 14. A linearly polarized light beam with its polarization along the LC alignment direction is incident onto the device. Due to the difference between the LC extraordinary refractive index (n_e) and the refractive index of polymer micro gratings (n_p), this polarized beam is deflected. The experimental results are shown in Figure 15a. The white light beam used here is unpolarized, so that the beam component with its polarization along the LC alignment is deflected, while the component with polarization perpendicular to the LC alignment is unaffected. The deflection angle is about 2.3° . When applying a strong electric field, most of the LC directors are realigned parallel to the field. The LC effective refractive index then approaches the ordinary one (n_o), which matches that of the micro gratings ($n_o = n_p$). The light component with its polarization parallel to the groove is therefore no longer deflected by the device. Thus, the whole unpolarized white light beam propagates along its original trace, as shown in Figure 15b. The deflection angle of the one-dimensional beam shaping device can be further improved by optimizing the grating structure, the LC, the polymer material, etc.

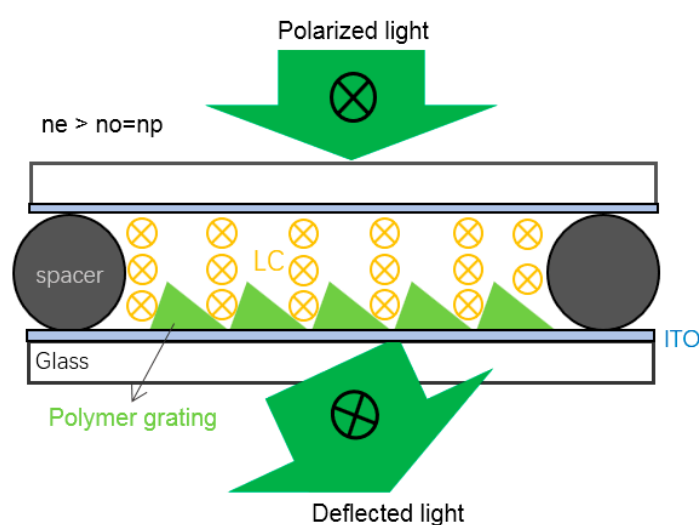


Figure 14. Schematic LC-micro grating device with one dimensional beam deflection; n_o —LC ordinary refractive index; n_e —LC extraordinary refractive index; n_p —refractive index of the polymer micro-structures.

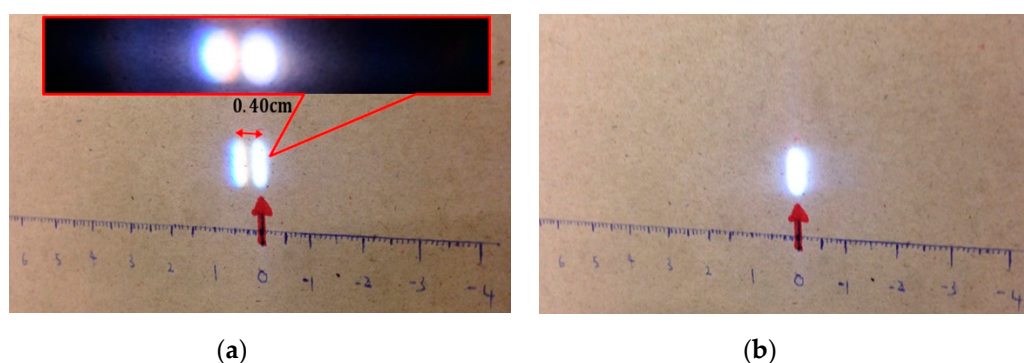


Figure 15. Beam deflection of an unpolarized white light beam by an LC-micro grating beam steering device with: (a) voltage-off, the inset gives a clearer view of white light beam deflection in a dark background; (b) voltage-on. Reproduced with permission [63]. Copyright 2015, IEEE.

3.2. Beam Broadening and Beam Condensing with LC-Circular Grating Devices

The beam shaping functionality is extended from one dimension to two dimensions in this section. Circular micro grating (CMG) structures are combined with nematic liquid crystals to realize the desired functionalities. Two kinds of optical components have been achieved: a LC beam expander and a LC beam condenser. Two CMG structures with reversed shapes are respectively fabricated

based on the same master mold using the soft lithography technology described above. Nematic LC E7 is used for the 2D switchable beam shaping components and the LC is initially aligned in an anti-parallel alignment.

The two CMG structures have the same dimension, but the grating units are oriented in reversed directions. The reversed grating profiles lead to two different beam shaping properties. The two LC devices work only for a linearly polarized light with its polarization along the initial LC alignment. Because the ordinary refractive index of E7 is chosen to equal that of the CMGs, the two devices demonstrate the beam broadening and beam condensing performance when there is no voltage applied, and the results are shown in Figure 16a,c, respectively. Upon the application of high voltages, the LC molecules reorient parallel to the electric field. The effective refractive index for the light propagating through the LC layer now equals that of the CMG structures, therefore the light beam passes through the two devices without any change, as demonstrated in Figure 16b,d.

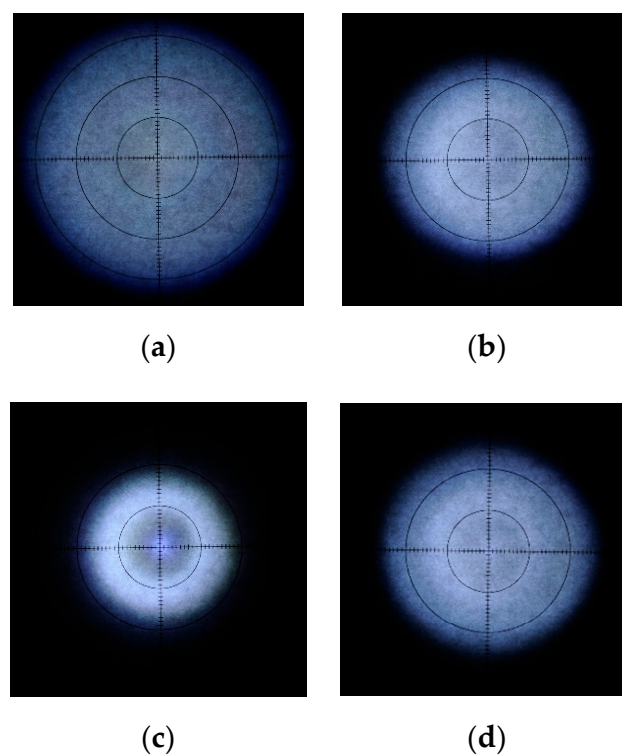


Figure 16. Circular beam shaping of LC-CMG devices with a white LED and a polarizer: (a) $V = 0 V_{pp}$ and (b) $V = 50 V_{pp}$ for the LC beam broadening device; (c) $V = 0 V_{pp}$ and (d) $V = 50 V_{pp}$ for the LC beam condensing device. Reproduced with permission [77]. Copyright 2016, IOP Publishing.

The curves of the FWHM (full width at half maximum) versus the applied voltage are obtained from the beam shaping patterns of the two LC devices, as shown in Figure 17. It is seen that the beam shaping pattern of the LC beam broadening device demonstrates a gradual decreasing trend by increasing the applied voltage, while the LC beam condensing device shows the opposite behavior: its FWHM is increased with increasing electric field. Due to the equal grating size and LC material, both LC devices deflect the light beam over 2° , but exert a different beam shaping effect on the original beam. The steering angles of these kinds of LC devices can be further improved by adopting new LC materials with a larger birefringence and grating units with a larger blaze angle. Moreover, polarization independent LC beam broadening or beam condensing components can be realized by stacking two single devices with their LC alignment orthogonal to each other. This scheme has been realized and it demonstrated good optical performance [77].

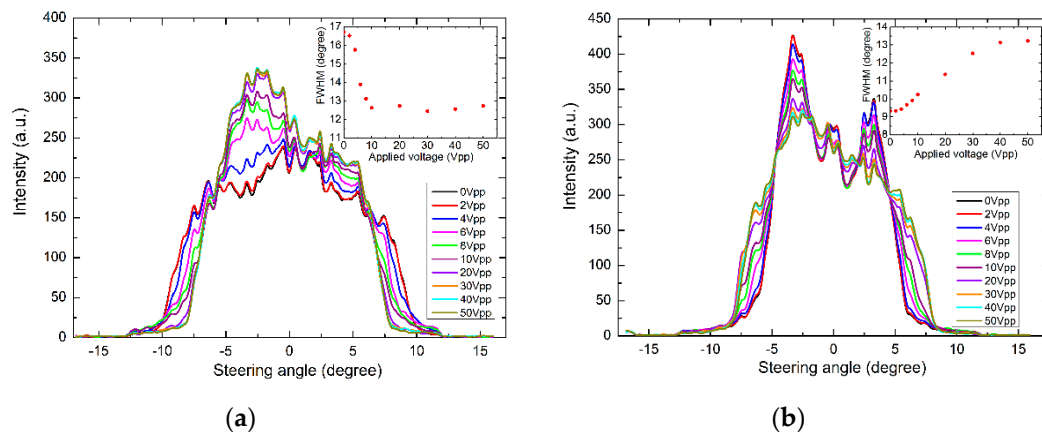


Figure 17. Plots of the intensity distribution as a function of angle for (a) LC beam broadening device and (b) LC beam condensing device. Reproduced with permission [77]. Copyright 2016, IOP Publishing.

3.3. Polarization Independent Beam Shaping Using a Ch LC-Micro Grating Device

An unpolarized light beam can always be decomposed into two linearly polarized beam components with mutually orthogonal polarizations. Polarization independent beam shaping is therefore possible by stacking two mutually orthogonal devices, since each single LC device will act on one of the two beam components. However, this has drawbacks, such as the increased thickness, higher cost, and more complex driving electronics. Therefore, single LC beam shaping devices with polarization independence are still in demand. Cholesteric (Ch) LCs have a helical structure whereby the layered LC molecules rotate around the helical axis with a pitch P_0 . If the helical axis orientation is uniform and perpendicular to the device substrate, the planar (P) state appears. This state exhibits a strong Bragg reflection at the wavelength $\lambda_p = n_{ave} \times P_0$ with n_{ave} the average refractive index between the ordinary (n_o) and the extraordinary (n_e) refractive index of the LC [86]. Due to the helical structure and complex nano structures with different orientations, the average refractive index experienced by the incident light in the P state is polarization independent. When a strong electric field is applied, the helical structures are unwound, and all LC molecules are realigned parallel to the field. This so-called homeotropic (H) state exhibits an effective refractive index that is always n_o for a normally incident light beam, regardless of its polarization. By combining micro grating structures with the two states of the Ch-LCs, switchable polarization independent beam deflection is expected to occur.

The Ch-LC material used for polarization independent beam shaping devices is composed of a nematic LC and a chiral dopant. The Bragg reflective wavelength is chosen in the infrared wavelength (IR) region, so that visible light can pass through the Ch-LC layer and be modulated by the device shown in Figure 18. The average refractive index of the Ch-LC is larger than that of the micro grating, while its ordinary refractive index matches that of the grating. Hence, in the P state, the device deflects an (unpolarized) light beam, while in the H state the beam passes without any deflection. The experimental results are demonstrated in Figure 19a,b, respectively. It is found that, upon removal of the strong electric field, the LC texture does not revert to the P state but changes into the focal conic (FC) state, resulting in strong light scattering, as shown in Figure 19c. The issue that the FC state does not switch back to the P state with conventional Ch-LCs, can be solved by using dual frequency Ch-LCs. Dual frequency Ch-LC consisting of dual frequency nematic LC (HEF951800-100) and chiral dopant (R5011) is used to replace the conventional Ch-LC. A high frequency voltage drives the FC state into the P state, therefore switchable beam steering is achieved between the P state and the H state.

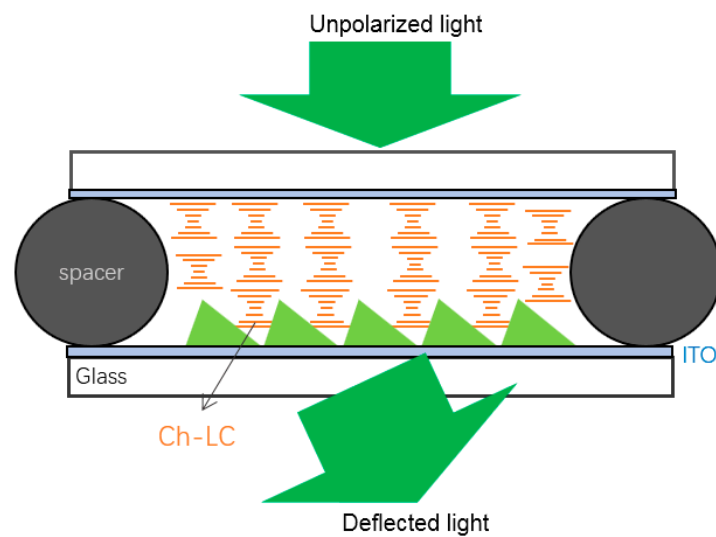


Figure 18. Schematic Ch-LC beam deflection device with polarization independence.

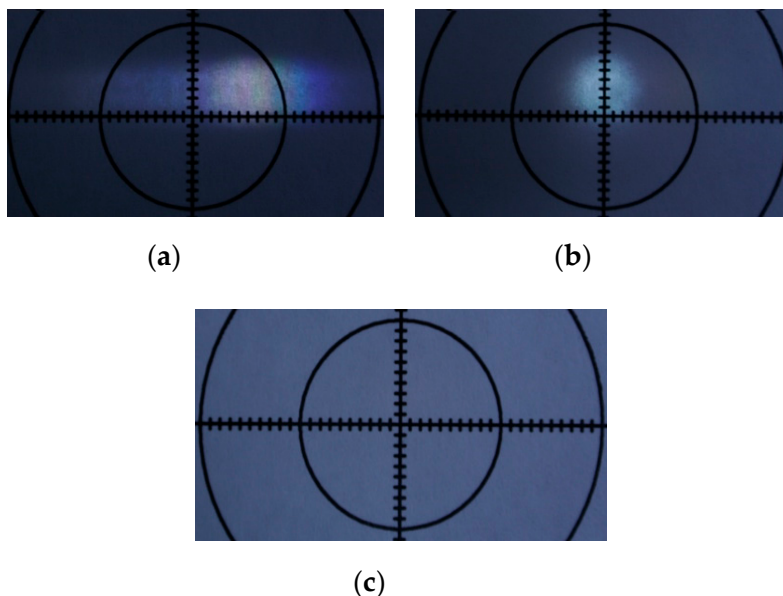


Figure 19. White light beam deflection by Ch-LC beam steering device: (a) P state; (b) H state; (c) FC state. Reproduced with permission [87]. Copyright 2017, Nature Publishing.

Polarization independence of the DF Ch-LC based beam steering components is verified by measuring the device transmittance for an incident light beam with a rotatable linear polarization. The results are shown in Figure 20 for four different LC alignment schemes:

Scheme 1—Bare grating rubbed along the grooves combined with flat ITO counterpart coated with a rubbed polyimide (PI) layer to form anti-parallel LC alignment.

Scheme 2—Bare grating rubbed along the grooves combined with flat ITO counterpart coated with a rubbed PI layer to form orthogonal LC alignment.

Scheme 3—Bare grating without rubbing combined with flat ITO counterpart coated with a non-rubbed PI layer.

Scheme 4—Bare grating without rubbing combined with bare flat ITO counterpart without a PI layer.

The lowest relative transmission fluctuation ratio (4.4%) is found for the scheme without alignment layer or rubbing (Scheme 4) as explained in [87]. The remaining polarization dependence is attributed

to the tilted nature of the electric fields if the transparent electrode is positioned on top of the grating structures. Moving the electrode below the grating structure reduces the tilt angle of the electric field and further diminish the polarization dependence at the expense of higher driving voltages, as confirmed by an experiment with a nematic LC-grating device as shown in Figure 20b.

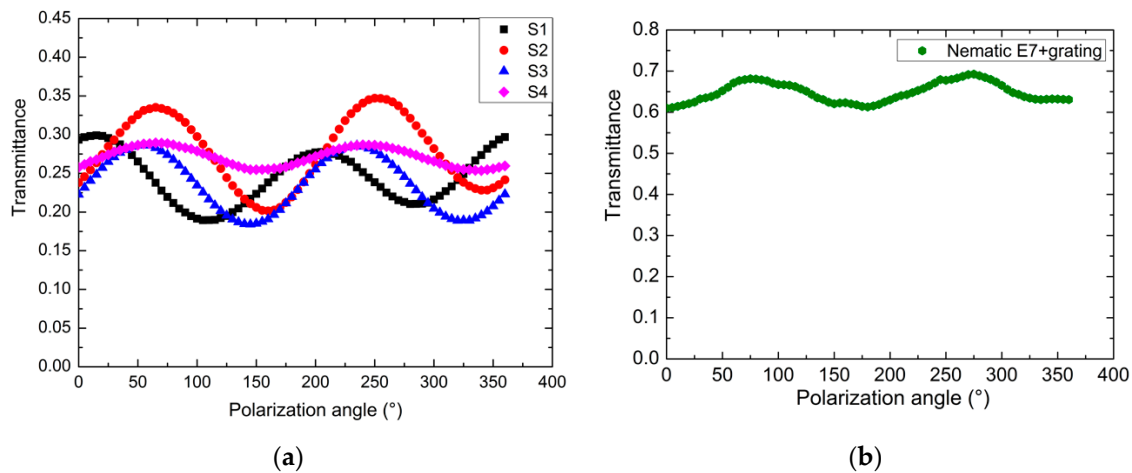


Figure 20. The transmission versus the polarizing angle of a polarizer: (a) for the P state of different Ch-LC beam steering devices; (b) for a NLC-grating device with applying $V_{app} = 600 V_{pp}$. Reproduced with permission [87]. Copyright 2017, Nature Publishing.

3.4. Fast Switching LC Beam Deflection Using Dual Frequency Driving

Dual-frequency (DF) Ch-LC is employed to switch the LC texture from the H or FC state to the P state in the above-mentioned section. This scheme can also be used to accelerate the LC switching and improve the device response behavior. Compared to the nematic LC devices, the response time of DF Ch-LC-grating beam steering components is significantly improved. However, the switching time is still in the range of hundreds of milliseconds and does not meet the demand of video displays with a frame duration of 16.7 ms. Therefore, dual frequency driving nematic LC beam shaping devices are proposed.

Figure 21 illustrates the working principle of the dual frequency driven nematic LC beam shaping component. Nematic DF LCs exhibit a positive dielectric anisotropy ($\Delta\epsilon$) in response to voltages with a low frequency. The LC molecules are aligned parallel to the applied electric field. When applying electric fields with high frequencies, the dielectric anisotropy becomes negative. The LC molecules with a negative $\Delta\epsilon$ reorient perpendicularly to the electric field, due to the net torque induced by the larger permittivity parallel to the short LC axis. Voltages with large magnitudes but different frequencies are applied to both switching processes. It is expected that the response time of the device will be reduced. The ordinary refractive index of the DF nematic LC is set to match the micro grating structure, so that there is no beam deflection when the LC molecules are aligned perpendicularly to the substrate by a high voltage with a low frequency, as shown in Figure 22. The main intensity is located on the -1 st order (50.4%), indicating that the LC ordinary refractive index still deviates from that of the polymer grating. When the low frequency is replaced by a high one, the LC directors are forced to lie down and the laser beam is deflected to the $+3$ rd (45.4%) and $+4$ th (10.5%) orders, due to the large refractive index difference between the LC extraordinary index and the grating index.

The response time of the DF nematic LC—micro-grating based beam deflecting component using dual frequency driving is measured for both the -1 st order and $+3$ rd order, respectively. It is found that the switching-on time (100 kHz \rightarrow 100 Hz) for the -1 st order is larger than for the $+3$ rd order, and the switching-off time (100 Hz \rightarrow 100 kHz) for the $+3$ rd order is larger than that for the -1 st order. The longer switching time is chosen for the characterization of the two switching processes, the results are shown in Figure 23. The switch-on time of the DF LC-grating device is 20.5 ms, while the switch-off

time is only 3.8 ms. The large difference in the switching times is attributed to the role of the LC elastic energy in the two processes: the initial LC alignment is homogenous, thus the LC elastic energy accelerates the switching back of LC molecules for the high frequency driving, while it hinders the deformation induced by the electric field with a low frequency. The total switching time is 24.3 ms and approaches the requirements for video frame rate applications.

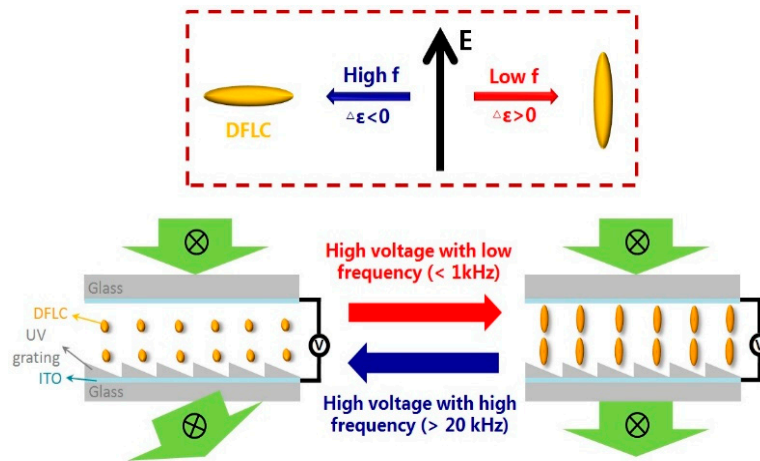


Figure 21. DFLC beam deflection device using dual frequency driving. Reproduced with permission [88]. Copyright 2019, IOP Publishing.

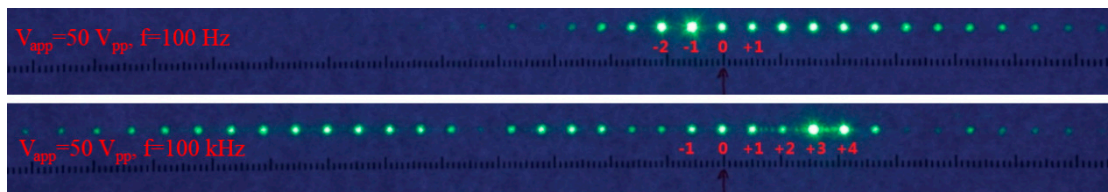


Figure 22. Laser beam deflection by the DF nematic LC beam deflector using dual frequency driving. Reproduced with permission [88]. Copyright 2019, IOP Publishing.

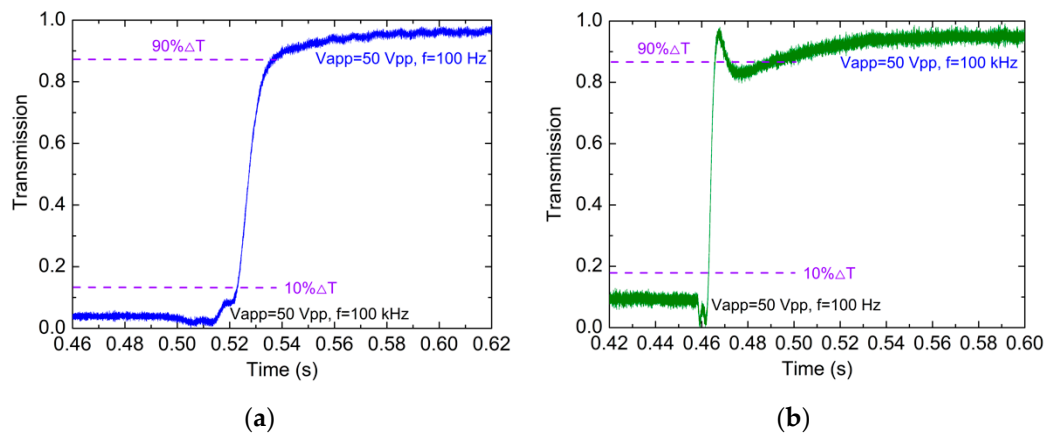


Figure 23. The switching time of the DF NLC beam steering device by applying $V_{app} = 50 V_{pp}$: (a) with $f = 100 \text{ kHz} \rightarrow 100 \text{ Hz}$; (b) with $f = 100 \text{ Hz} \rightarrow 100 \text{ kHz}$. Reproduced with permission [88]. Copyright 2019, IOP Publishing.

3.5. Blue Phase LC-Micro Grating Based Beam Steering Device

Blue phase (BP) LCs usually appear between the chiral nematic LC state and the isotropic state of specific highly chiral LCs. Generally, BPLCs have crystal-like structures, which are composed of double twisted cylinders. Pure BPLCs normally exist only within a very narrow temperature interval

of a few degrees Celsius, but polymer stabilized (PS) BPLCs demonstrate a much broader temperature range including room temperature. BPLCs have some unique advantages, such as sub-millisecond response times and the absence of the need for alignment layers [89,90], which make them applicable to fast response systems with a simple device architecture.

The PS-BPLC is combined with micro grating structures to realize faster response beam shaping components, compared to the aforementioned beam shaping devices using dual-frequency nematic LC. The device structure is depicted in Figure 24.

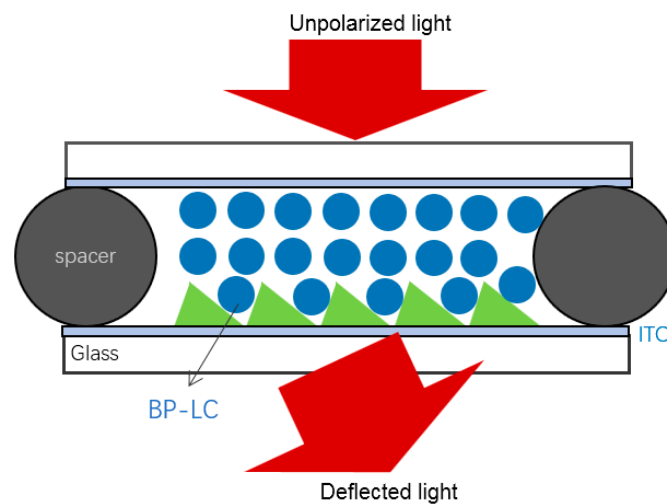


Figure 24. Schematic BP LC-micro grating based beam steering device.

Without an electric field, the PS-BPLC behaves as a macroscopically isotropic material. Its refractive index is the averaged value between the ordinary and the extraordinary refractive index of the LC. If there is a refractive index mismatch between the isotropic state and the grating structure, the incident light will be deflected. The refractive index ellipsoid for the isotropic state can be represented by a sphere. This refractive index sphere is polarization independent, therefore the BP LC beam steering device shows polarization independence in the voltage-off state. When applying a strong electric field, the BP LC shows an elongated refractive index ellipsoid induced by the field. The incident light with various polarizations experiences the same refractive index as the ordinary ray, which equals the polymer grating index, it thus passes through the BPLC device without any deflection.

Figure 25 shows the beam deflection of the PSBP LC-grating beam steering device. It is observed that the diffraction intensity is mainly located on the -1 st and 0 th order without applied voltages. When applying 600 volts, the diffraction intensity is redistributed, and the main intensity goes to the 0 th and $+1$ st order. The small difference in the beam deflection is attributed to the low magnitude of the field induced birefringence of PSBP LCs, which can be solved by using an optimized PSBP LC and micro grating structure with a larger blaze angle. The response time of the PSBP LC-grating device is measured and shown in Figure 26. The response time of the switching-on and the switching-off is 1.61 ms and 1.70 ms, respectively. The device response is much faster than the dual frequency driving NLC beam steering components.

To verify the polarization independence of the PS BPLC-grating device, light beams with different polarization states are incident onto the device. The transmission curves with varied voltages are almost overlapping for different light beam polarizations (shown in Figure 27), indicating that the PSBP LC-grating beam steering components are polarization independent.

Polarization independent and fast response beam shaping is achieved by the PSBP LC-micro grating components.

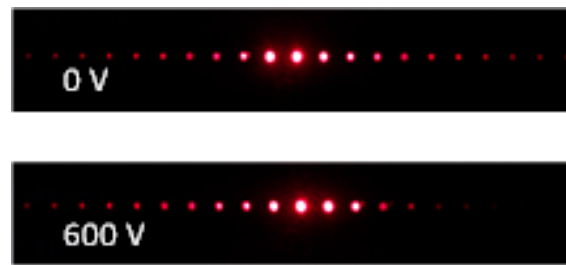


Figure 25. Laser beam ($\lambda = 633$ nm) steering patterns without and with applied voltages. Reproduced with permission [91]. Copyright 2017, Photonics Society of Poland.

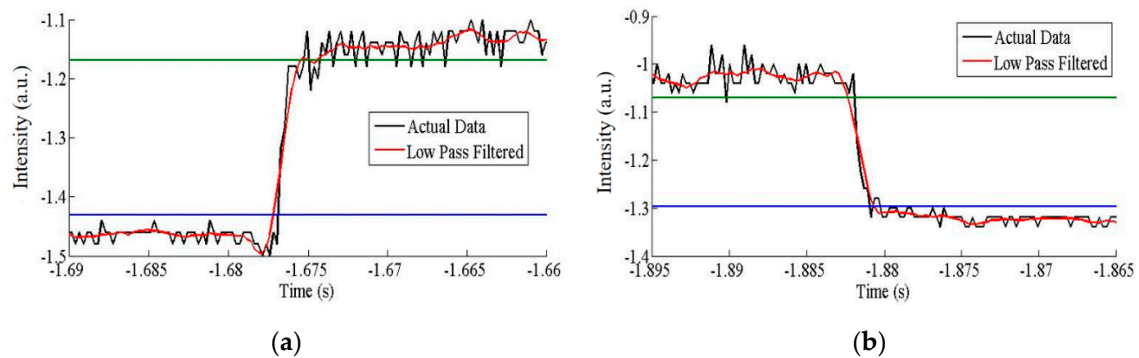


Figure 26. Response time of the PSBP LC-grating device measured at the 0th diffraction order: (a) switching on; (b) switching off. Reproduced with permission [91]. Copyright 2017, Photonics Society of Poland.

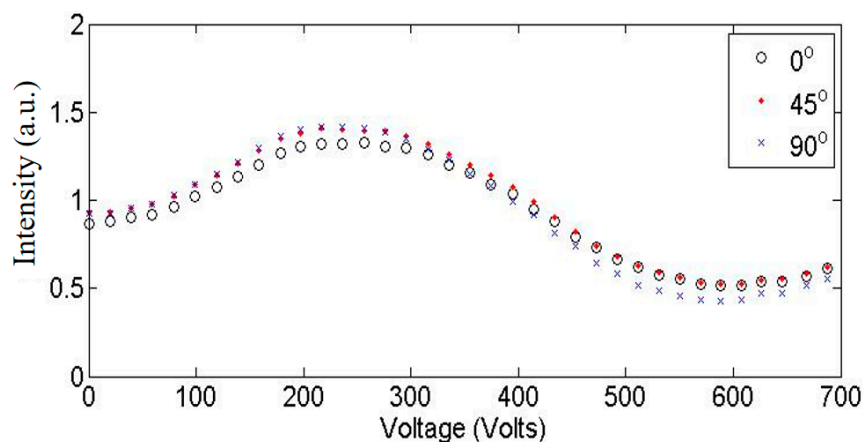


Figure 27. Intensity variation versus applied voltage for the 0th diffraction order of the PSBP LC-grating device with three different linearly polarized light beams. Reproduced with permission [91]. Copyright 2017, Photonics Society of Poland.

4. Conclusions

The recent development of LC beam shaping devices for active optical manipulation is discussed and reviewed in this work. The advances in modern optic design methods and optical component fabrication technologies increase the importance of beam shaping devices based on LCs combined with micro optical structures. Different state-of-the-art techniques for optical micro structure fabrication are discussed with experimental results, and their characteristics are revealed: diamond tooling for complex shapes, laser ablation for less complex structures but in a relatively rapid way, hot embossing for rapid structure replications in thick thermoplastics, and soft lithography for rapid and thin layered structure replications. Optical micro-structures are combined with different LC materials to realize a variety of LC operation modes and these lead to various beam shaping functionalities, ranging from

one-dimensional beam deflection to two-dimensional beam shaping, from polarization dependent to polarization independent, from slow response to fast response, etc. The LC-microstructure based beam shaping components discussed in this work have supplied the field with novel ideas, new knowledge and advanced technologies, paving the way for novel applications of LC beam shaping devices.

Author Contributions: Conceptualization, X.S., D.C. and T.B.; methodology, X.S., M.V. and J.B.; validation, X.S., M.V. and T.B.; resources, H.D.S., K.N. and H.T.; data curation, X.S. and Q.L.; writing—original draft preparation, X.S., T.B. and H.D.S.; writing—review and editing, H.D.S. and C.W.; supervision, H.L. and C.J.; project administration, H.D.S. and H.L.; funding acquisition, H.D.S., H.T., K.N. and H.L. All authors have read and agreed to the published version of the manuscript.

Funding: This study was partly supported by the Agency for Innovation by Science and Technology (IWT) through the SBO project SECONDOS (nr 120019), partly by the Research Foundation Flanders (FWO) through the project G.A047.11N, partly by the National Natural Science Foundation of China (Grant No. 11774057), partly by the Fundamental Research Funds for the Central Universities (Grant No. 20153638), and partly by the China Postdoctoral Science Foundation (Grant No. 2019M651573).

Acknowledgments: We thank the Hercules Foundation for providing funding for the APPLIE4MOS polymer prototyping line used in this research.

Conflicts of Interest: The authors declare no conflict of interest. The funders had no role in the design of the study; in the collection, analyses, or interpretation of data; in the writing of the manuscript, or in the decision to publish the results.

References

1. Santiago-Alvarado, A.; Vazquez-Montiel, S.; Gonzalez-Garcia, J.; Iturbide-Jimenez, F.; Cruz-Felix, A.S.; Cruz-Martinez, V.; Lopez-Lopez, E.A.; Castro-Gonzalez, G. Advances in the development of tunable lenses in Mexico. *Photon. Lett. Pol.* **2015**, *7*, 20–22. [[CrossRef](#)]
2. Tapos, F.M.; Edinger, D.J.; Hilby, T.R.; Ni, M.S.; Holmes, B.C.; Stubbs, D.M. High bandwidth fast steering mirror. *Opt. Photon.* **2005**, *5877*, 587707. [[CrossRef](#)]
3. Yoder, P.; Vukobratovich, D. *Opto-Mechanical Systems Design*, 4th ed.; CRC Press: Boca Raton, FL, USA, 2015; pp. 1–46.
4. Torres, D.; Dooley, S.; Starman, L.A. Large Out-of-Plane Deflection MEMS Actuators for Optical Applications. *Proceedings* **2018**, *2*, 1072. [[CrossRef](#)]
5. Pengwang, E.; Rabenoroso, K.; Rakotondrabe, M.; Andreff, N. Scanning Micromirror Platform Based on MEMS Technology for Medical Application. *Micromachines* **2016**, *7*, 24. [[CrossRef](#)] [[PubMed](#)]
6. Sabry, Y.; Khalil, D.; Saadany, B.; Bourouina, T. Wide steering angle microscanner based on curved surface. *Proc. SPIE* **2013**, *8616*, 86160.
7. Chan, T.K.; Megens, M.; Yoo, B.W.; Wyras, J.; Chang-Hasnain, C.J.; Wu, M.C.; Horsley, D.A. Optical beam steering using an 8×8 mems phased array with closed-loop interferometric phase control. *Opt. Express* **2013**, *21*, 2807–2815. [[CrossRef](#)] [[PubMed](#)]
8. Lee, C.-C.; Ting, Y.-S.; Fang, W. Development of passive and active microprism arrays to change the radiation pattern of solid-state lighting. *J. Micromech. Microeng.* **2012**, *22*, 105038. [[CrossRef](#)]
9. Tuantranont, A.; Bright, V.; Zhang, J.; Zhang, W.; Neff, J.; Lee, Y. Optical beam steering using MEMS-controllable microlens array. *Sens. Actuators A Phys.* **2001**, *91*, 363–372. [[CrossRef](#)]
10. Krogmann, F.; Mönch, W.; Zappe, H. A MEMS-based variable micro-lens system. *J. Opt. A Pure Appl. Opt.* **2006**, *8*, 330–336. [[CrossRef](#)]
11. Nabil, G.; Ho, W.F.; Chan, H.P. Experimental study on the performance of a variable optical attenuator using polymer dispersed liquid crystal. *Appl. Opt.* **2013**, *52*, 15–21. [[CrossRef](#)] [[PubMed](#)]
12. Cheng, H.; Bhowmik, A.; Bos, P.J. Fast-response liquid crystal variable optical retarder and multilevel attenuator. *Opt. Eng.* **2013**, *52*, 107105. [[CrossRef](#)]
13. Huh, J.-W.; Yu, B.-H.; Heo, J.; Ji, S.-M.; Yoon, T.-H. Technologies for display application of liquid crystal light shutters. *Mol. Cryst. Liq. Cryst.* **2017**, *644*, 120–129. [[CrossRef](#)]
14. Fells, J.A.; Wang, X.; Elston, S.J.; Welch, C.; Mehl, G.H.; Booth, M.; Morris, S.M. Flexoelectro-optic liquid crystal analog phase-only modulator with a 2π range and 1 kHz switching. *Opt. Lett.* **2018**, *43*, 4362–4365. [[CrossRef](#)] [[PubMed](#)]

15. Caño-García, M.; Quintana, X.; Otón, J.M.; Geday, M.A. Dynamic multilevel spiral phase plate generator. *Sci. Rep.* **2018**, *8*, 15804. [[CrossRef](#)] [[PubMed](#)]
16. Choi, M. Universal phase-only spatial light modulators. *Opt. Express* **2017**, *25*, 22253. [[CrossRef](#)]
17. Oton, E.; Netter, E. Wide tunable shift of the reflection band in dual frequency cholesteric liquid crystals. *Opt. Express* **2017**, *25*, 13314. [[CrossRef](#)]
18. Oton, J.M.; Caño-García, M.; Gordo, F.; Otón, E.; Geday, M.A.; Quintana, X. Liquid crystal tunable claddings for polymer integrated optical waveguides. *Beilstein J. Nanotechnol.* **2019**, *10*, 2163–2170. [[CrossRef](#)]
19. Abuleil, M.J.; Abdulhalim, I. Narrowband multispectral liquid crystal tunable filter. *Opt. Lett.* **2016**, *41*, 1957–1960. [[CrossRef](#)]
20. Otón, J.M.; Otón, E.; Quintana, X.; Geday, M.A. Liquid-crystal phase-only devices. *J. Mol. Liq.* **2018**, *267*, 469–483. [[CrossRef](#)]
21. Algorri, J.F.; Urruchi, V.; Bennis, N.; Oton, J.M.; Otón, J.M. Tunable liquid crystal cylindrical micro-optical array for aberration compensation. *Opt. Express* **2015**, *23*, 13899–13915. [[CrossRef](#)]
22. Stebryte, M.; Nys, I.; Ussembayev, Y.Y.; Beeckman, J.; Neyts, K. Large Angle Forward Diffraction by Chiral Liquid Crystal Gratings with Inclined Helical Axis. *Crystals* **2020**, *10*, 807. [[CrossRef](#)]
23. Chao, P.C.-P.; Kao, Y.-Y.; Hsu, C.-J. A new negative liquid crystal lens with multiple ring electrodes in unequal widths. *IEEE Photon. J.* **2012**, *4*, 250–266. [[CrossRef](#)]
24. Kim, J.; Oh, C.; Serati, S.; Escuti, M.J. Wide-angle, nonmechanical beam steering with high throughput utilizing polarization gratings. *Appl. Opt.* **2011**, *50*, 2636–2639. [[CrossRef](#)]
25. Xiang, X.; Kim, J.; Escuti, M.J. Bragg polarization gratings for wide angular bandwidth and high efficiency at steep deflection angles. *Sci. Rep.* **2018**, *8*, 1–6. [[CrossRef](#)] [[PubMed](#)]
26. Algorri, J.F.; Urruchi, V.; Bennis, N.; Morawiak, P.; Sánchez-Pena, J.M.; Otón, J.M.; Oton, J.M. Liquid crystal spherical microlens array with high fill factor and optical power. *Opt. Express* **2017**, *25*, 605. [[CrossRef](#)]
27. Oton, E.; Morawiak, P.; Mazur, R.; Quintana, X.; Geday, M.A.; Oton, J.M.; Piecek, W. Diffractive and Refractive Liquid Crystal Devices Based on Multilayer Matrices. *J. Light. Technol.* **2019**, *37*, 2086–2093. [[CrossRef](#)]
28. Yousefzadeh, C.; Van Rynbach, A.; Bos, P.J. Design of a large aperture, tunable, Pancharatnam phase beam steering device. *Opt. Express* **2020**, *28*, 991–1001. [[CrossRef](#)]
29. Li, L.; Bryant, D.; Van Heugten, T.; Bos, P.J. Near-diffraction-limited and low-haze electro-optical tunable liquid crystal lens with floating electrodes. *Opt. Express* **2013**, *21*, 8371–8381. [[CrossRef](#)] [[PubMed](#)]
30. Geday, M.A.; Caño-García, M.; Otón, J.M.; Quintana, X. Adaptive Spiral Diffractive Lenses—Lenses with a Twist. *Adv. Opt. Mater.* **2020**, 2001199, 1–5. [[CrossRef](#)]
31. Willekens, O.; George, J.P.; Neyts, K.; Beeckman, J. Ferroelectric thin films with liquid crystal for gradient index applications. *Opt. Express* **2016**, *24*, 8088. [[CrossRef](#)]
32. Klaus, W.; Ide, M.; Morokawa, S.; Tsuchiya, M.; Kamiya, T. Angle-independent beam steering using a liquid crystal grating with multi-resistive electrodes. *Opt. Commun.* **1997**, *138*, 151–157. [[CrossRef](#)]
33. Naumov, A.F.; Loktev, M.Y.; Guralnik, I.R.; Vdovin, G. Liquid-crystal adaptive lenses with modal control. *Opt. Lett.* **1998**, *23*, 992–994. [[CrossRef](#)]
34. Shang, X.; Trinidad, A.M.; Joshi, P.; De Smet, J.; Cuypers, D.; De Smet, H. Tunable Optical Beam Deflection Via Liquid Crystal Gradient Refractive Index Generated by Highly Resistive Polymer Film. *IEEE Photon. J.* **2016**, *8*, 1–11. [[CrossRef](#)]
35. Asatryan, K.; Presnyakov, V.; Tork, A.; Zohrabyan, A.; Bagramyan, A.; Galstian, T. Optical lens with electrically variable focus using an optically hidden dielectric structure. *Opt. Express* **2010**, *18*, 13981–13992. [[CrossRef](#)] [[PubMed](#)]
36. Ren, H.; Fan, Y.-H.; Wu, S.-T. Polymer network liquid crystals for tunable microlens arrays. *J. Phys. D Appl. Phys.* **2004**, *37*, 400–403. [[CrossRef](#)]
37. Ren, H.; Wu, S.-T. Tunable electronic lens using a gradient polymer network liquid crystal. *Appl. Phys. Lett.* **2003**, *82*, 22–24. [[CrossRef](#)]
38. Ren, H.; Xu, S.; Wu, S.-T. Polymer-stabilized liquid crystal microlens array with large dynamic range and fast response time. *Opt. Lett.* **2013**, *38*, 3144–3147. [[CrossRef](#)]
39. Xu, S.; Li, Y.; Liu, Y.; Sun, J.; Ren, H.; Wu, S.-T. Fast-Response Liquid Crystal Microlens. *Micromachines* **2014**, *5*, 300–324. [[CrossRef](#)]
40. Ren, H.; Xu, S.; Wu, S.-T. Gradient polymer network liquid crystal with a large refractive index change. *Opt. Express* **2012**, *20*, 26464–26472. [[CrossRef](#)]

41. Sun, J.; Xu, S.; Ren, H.; Wu, S.-T. Reconfigurable fabrication of scattering-free polymer network liquid crystal prism/grating/lens. *Appl. Phys. Lett.* **2013**, *102*, 161106. [[CrossRef](#)]
42. Khorasaninejad, M.; Chen, W.T.; Devlin, R.C.; Oh, J.; Zhu, A.Y.; Capasso, F. Metalenses at visible wavelengths: Diffraction-limited focusing and subwavelength resolution imaging. *Science* **2016**, *352*, 1190–1194. [[CrossRef](#)] [[PubMed](#)]
43. Khorasaninejad, M.; Chen, W.T.; Oh, J.; Capasso, F. Super-Dispersive Off-Axis Meta-Lenses for Compact High Resolution Spectroscopy. *Nano Lett.* **2016**, *16*, 3732–3737. [[CrossRef](#)] [[PubMed](#)]
44. Zhao, Y.; Alù, A. Tailoring the Dispersion of Plasmonic Nanorods To Realize Broadband Optical Meta-Waveplates. *Nano Lett.* **2013**, *13*, 1086–1091. [[CrossRef](#)] [[PubMed](#)]
45. Anandan, J. The geometric phase. *Nat. Cell Biol.* **1992**, *360*, 307–313. [[CrossRef](#)]
46. Hasman, E.; Kleiner, V.; Biener, G.; Niv, A. Polarization dependent focusing lens by use of quantized Pancharatnam–Berry phase diffractive optics. *Appl. Phys. Lett.* **2003**, *82*, 328–330. [[CrossRef](#)]
47. Yu, N.; Genevet, P.; Kats, M.A.; Aieta, F.; Tetienne, J.-P.; Capasso, F.; Gaburro, Z. Light Propagation with Phase Discontinuities: Generalized Laws of Reflection and Refraction. *Science* **2011**, *334*, 333–337. [[CrossRef](#)]
48. Kim, J.; Li, Y.; Miskiewicz, M.N.; Oh, C.; Kudenov, M.W.; Escuti, M.J. Fabrication of ideal geometric-phase holograms with arbitrary wavefronts. *Optica* **2015**, *2*, 958–964. [[CrossRef](#)]
49. Ma, Y.; Tam, A.M.W.; Gan, X.T.; Shi, L.Y.; Srivastava, A.K.; Chigrinov, V.G.; Kwok, H.S.; Zhao, J.L. Fast switching ferroelectric liquid crystal Pancharatnam–Berry lens. *Opt. Express* **2019**, *27*, 10079–10086. [[CrossRef](#)]
50. Shi, Y.; Lai, Y.; Liu, Y.; Chigrinov, V.G.; Kwok, H.-S.; Hu, M.; Luo, D.; Sun, X.W. Two-dimensional liquid crystal polarization grating via linearly polarized light modified multi-beam polarization interferometry. *Opt. Express* **2019**, *27*, 13061–13071. [[CrossRef](#)]
51. Zhou, Y.; Yin, Y.; Yuan, Y.; Lin, T.; Huang, H.; Yao, L.; Wang, X.; Tam, A.M.W.; Fan, F.; Wen, S. Liquid crystal Pancharatnam–Berry phase lens with spatially separated focuses. *Liq. Cryst.* **2018**, *46*, 995–1000. [[CrossRef](#)]
52. Flack, J.; Harrold, J.; Woodgate, G.J. A prototype 3D mobile phone equipped with a next-generation autostereoscopic display. *Proc. SPIE* **2007**, *6490*, 64900M. [[CrossRef](#)]
53. Kim, J.; Miskiewicz, M.N.; Serati, S.; Escuti, M.J. Nonmechanical Laser Beam Steering Based on Polymer Polarization Gratings: Design Optimization and Demonstration. *J. Light. Technol.* **2015**, *33*, 2068–2077. [[CrossRef](#)]
54. Ren, H.; Xu, S.; Liu, Y.; Wu, S.-T. Switchable focus using a polymeric lenticular microlens array and a polarization rotator. *Opt. Express* **2013**, *21*, 7916–7925. [[CrossRef](#)]
55. Krijn, M.P.C.M.; De Zwart, S.T.; De Boer, D.K.G.; Willemsen, O.H.; Sluijter, M. 2-D/3-D displays based on switchable lenticulars. *J. Soc. Inf. Disp.* **2008**, *16*, 847–885. [[CrossRef](#)]
56. Choi, Y.; Park, J.-H.; Kim, J.-H.; Lee, S.-D. Fabrication of a focal length variable microlens array based on a nematic liquid crystal. *Opt. Mater.* **2003**, *21*, 643–646. [[CrossRef](#)]
57. Shang, X.; Desmet, A.; Joshi, P.; De Smet, J.; Cuypers, D.; De Smet, H. 68–2: Smart Liquid Crystal Beam Deflector With Laser Ablated Polymer Micro Grating Structure. *SID Symp. Dig. Tech. Pap.* **2016**, *47*, 931–933. [[CrossRef](#)]
58. Reznikov, M.; Reznikov, Y.; Slyusarenko, K.; Varshal, J.; Manevich, M. Adaptive properties of a liquid crystal cell with a micro lens profiled aligning surface. *J. Appl. Phys.* **2012**, *111*, 103118. [[CrossRef](#)]
59. Commander, L.; Day, S.; Selviah, D. Variable focal length microlenses. *Opt. Commun.* **2000**, *177*, 157–170. [[CrossRef](#)]
60. Wang, X.; Wilson, D.; Muller, R.; Maker, P.; Psaltis, D. Liquid-crystal blazed-grating beam deflector. *Appl. Opt.* **2000**, *39*, 6545–6555. [[CrossRef](#)]
61. Ren, H.; Fan, Y.-H.; Lin, Y.-H.; Wu, S.-T. Tunable-focus microlens arrays using nanosized polymer-dispersed liquid crystal droplets. *Opt. Commun.* **2005**, *247*, 101–106. [[CrossRef](#)]
62. Hwang, S.J.; Liu, Y.X.; Porter, G.A. Improvement of performance of liquid crystal microlens with polymer surface modification. *Opt. Express* **2014**, *22*, 4620–4627. [[CrossRef](#)] [[PubMed](#)]
63. Shang, X.; Tan, J.-Y.; Willekens, O.; De Smet, J.; Joshi, P.; Cuypers, D.; Islamaj, E.; Beeckman, J.; Neyts, K.; Vervaeke, M.; et al. Electrically Controllable Liquid Crystal Component for Efficient Light Steering. *IEEE Photon. J.* **2015**, *7*, 1–13. [[CrossRef](#)]
64. Willekens, O.; Jia, X.; Vervaeke, M.; Shang, X.; Baghdasaryan, T.; Thienpont, H.; De Smet, H.; Neyts, K.; Beeckman, J. Reflective liquid crystal hybrid beam-steerer. *Opt. Express* **2016**, *24*, 21541–21550. [[CrossRef](#)] [[PubMed](#)]

65. Karow, H.H. *Fabrication Methods for Precision Optics*; John Wiley and Sons: New York, NY, USA, 1993; pp. 610–680.
66. Bennett, H.E.; Porteus, J.O. Relation Between Surface Roughness and Specular Reflectance at Normal Incidence. *J. Opt. Soc. Am.* **1961**, *51*, 123–129. [[CrossRef](#)]
67. Dlott, D.D. Ultrafast vibrational energy transfer in the real world: Laser ablation, energetic solids, and hemeproteins. *J. Opt. Soc. Am. B* **1990**, *7*, 1638–1652. [[CrossRef](#)]
68. Soběhart, J.R. Polyimide ablation using intense laser beams. *J. Appl. Phys.* **1993**, *74*, 2830–2833. [[CrossRef](#)]
69. Keyes, T.; Clarke, R.H.; Isner, J.M. Theory of photoablation and its implications for laser phototherapy. *J. Phys. Chem.* **1985**, *89*, 4194–4196. [[CrossRef](#)]
70. Davis, G.M.; Gower, M.C. Time resolved transmission studies of poly (methyl methacrylate) films during ultraviolet laser ablative photodecomposition. *J. Appl. Phys.* **1987**, *61*, 2090–2092. [[CrossRef](#)]
71. Bitururin, N.; Luk'yanchuk, B.S.; Hong, M.H.; Chong, T.C. Models for laser ablation of polymers. *Chem. Rev.* **2003**, *103*, 519–552. [[CrossRef](#)]
72. Brannon, J.H.; Scholl, D.; Kay, E. Ultraviolet photoablation of a plasma-synthesized fluorocarbon polymer. *Appl. Phys. A* **1991**, *52*, 160–166. [[CrossRef](#)]
73. Zweig, A.D.; Venugopalan, V.; Deutsch, T.F. Stress generated in polyimide by excimer-laser irradiation. *J. Appl. Phys.* **1993**, *74*, 4181–4189. [[CrossRef](#)]
74. Shang, X.; Desmet, A.; De Smet, J.; Joshi, P.; Cuypers, D.; Van Put, S.; Van Steenberge, G.; Vervaeke, M.; Thienpont, H.; De Smet, H. Laser ablation of micro-photonic structures for efficient light collection and distribution. *J. Phys. D Appl. Phys.* **2015**, *48*, 245101. [[CrossRef](#)]
75. Desmet, L.; Van Overmeire, S.; Van Erps, J.; Ottevaere, H.; Debaes, C.; Thienpont, H. Elastomeric inverse moulding and vacuum casting process characterization for the fabrication of arrays of concave refractive microlenses. *J. Micromech. Microeng.* **2006**, *17*, 81–88. [[CrossRef](#)]
76. Shang, X.; Missinne, J.; Beneitez, N.T.; Jablonski, M.; De Smet, J.; Joshi, P.; Cuypers, D.; Baghdasaryan, T.; Vervaeke, M.; Thienpont, H.; et al. Reverse Replication of Circular Micro Grating Structures with Soft Lithography. *Proc. SPIE* **2015**, *9661*, 96610.
77. Shang, X.; Joshi, P.; Tan, J.-Y.; De Smet, J.; Cuypers, D.; Baghdasaryan, T.; Vervaeke, M.; Thienpont, H.; De Smet, H. Switchable circular beam deflectors. *J. Phys. D Appl. Phys.* **2016**, *49*, 165101. [[CrossRef](#)]
78. Kim, J.-H.; Yoneya, M.; Yamamoto, J.; Yokoyama, H. Nano-rubbing of a liquid crystal alignment layer by an atomic force microscope: A detailed characterization. *Nanotechnology* **2002**, *13*, 133–137. [[CrossRef](#)]
79. Knorr, T.G.; Hoffman, R.W. Dependence of Geometric Magnetic Anisotropy in Thin Iron Films. *Phys. Rev.* **1959**, *113*, 1039–1046. [[CrossRef](#)]
80. Smith, D.O. Anisotropy in Permalloy Films. *J. Appl. Phys.* **1959**, *30*, S264–S265. [[CrossRef](#)]
81. Barbero, G.; Dozov, I.; Palierne, J.F.; Durand, G. Order Electricity and Surface Orientation in Nematic Liquid Crystals. *Phys. Rev. Lett.* **1986**, *56*, 2056–2059. [[CrossRef](#)]
82. Oton, E.; López-Andrés, S.; Bennis, N.; Oton, J.; Geday, M.A. Silicon oxides as alignment surfaces for vertically-aligned nematics in photonic devices. *Opto-Electron. Rev.* **2014**, *22*, 92–100. [[CrossRef](#)]
83. Gibbons, W.M.; Shannon, P.J.; Sun, S.-T.; Swetlin, B.J. Surface-mediated alignment of nematic liquid crystals with polarized laser light. *Nat. Cell Biol.* **1991**, *351*, 49–50. [[CrossRef](#)]
84. Miyachi, K.; Kobayashi, K.; Yamada, Y.; Mizushima, S. The world's first photo alignment LCD technology applied to generation ten factory. *SID Symp. Dig. Tech. Pap.* **2010**, *41*, 579–582. [[CrossRef](#)]
85. Chigrinov, V.; Muravski, A.; Kwok, H.S.; Takada, H.; Akiyama, H.; Takatsu, H. Anchoring properties of photoaligned azo-dye materials. *Phys. Rev. E* **2003**, *68*, 061702. [[CrossRef](#)] [[PubMed](#)]
86. Dreher, R.; Meier, G.; Saupe, A. Selective Reflection by Cholesteric Liquid Crystals. *Mol. Cryst. Liq. Cryst.* **1971**, *13*, 17–26. [[CrossRef](#)]
87. Shang, X.; Meeus, L.; Cuypers, D.; De Smet, H. Fast switching cholesteric liquid crystal optical beam deflector with polarization independence. *Sci. Rep.* **2017**, *7*, 6492. [[CrossRef](#)] [[PubMed](#)]
88. Shang, X.; Cuypers, D.; Chen, F.; Xu, C.; Li, Q.; Wu, C.; Li, H.; Jiang, C.; De Smet, H. Dual-frequency liquid crystal-polymer grating for fast response optical beam steering. *Smart Mater. Struct.* **2019**, *28*, 105036. [[CrossRef](#)]
89. Kikuchi, H.; Yokota, M.; Hisakado, Y.; Yang, H.; Kajiyama, T. Polymer-stabilized liquid crystal blue phases. *Nat. Mater.* **2002**, *1*, 64–68. [[CrossRef](#)]

90. Castles, F.; Day, F.V.; Morris, S.M.; Ko, D.-H.; Gardiner, D.J.; Qasim, M.M.; Nosheen, S.; Hands, P.J.W.; Choi, S.S.; Friend, R.H.; et al. Blue-phase templated fabrication of three-dimensional nanostructures for photonic applications. *Nat. Mater.* **2012**, *11*, 599–603. [[CrossRef](#)]
91. Joshi, P.; Willekens, O.; Shang, X.; De Smet, J.; Cuypers, D.; Van Steenberge, G.; Beeckman, J.; Neyts, K.; De Smet, H. Tunable light beam steering device using polymer stabilized blue phase liquid crystals. *Photon. Lett. Pol.* **2017**, *9*, 11. [[CrossRef](#)]

Publisher’s Note: MDPI stays neutral with regard to jurisdictional claims in published maps and institutional affiliations.



© 2020 by the authors. Licensee MDPI, Basel, Switzerland. This article is an open access article distributed under the terms and conditions of the Creative Commons Attribution (CC BY) license (<http://creativecommons.org/licenses/by/4.0/>).